Identifying and targeting the Mg-Fe-PmrAB regulatory circuit reverses phosphate starvation-driven polymyxin resistance in *Enterobacteriaceae*

Guangming Zhang,[1] Ziqing Deng,[1,6,8] Jiezhang Jiang,[2,3,8] Minji Wang,[1,7] Xiaoyuan Wang,[4,5,*] Xiaoyun Liu,[2,3,*] Aixin Yan[1,9,*]

[1]School of Biological Sciences, Faculty of Science, The University of Hong Kong, Hong Kong SAR, China

[2]Department of Microbiology and Infectious Disease Center, NHC Key Laboratory of Medical Immunology, School of Basic Medical Sciences, Peking University Health Science Center, Beijing, China

[3]Department of Infectious Diseases, Peking University Third Hospital, Beijing, China

[4]State Key Laboratory of Food Science and Resources, Jiangnan University, Wuxi, China

[5]School of Biotechnology, Jiangnan University, Wuxi, China

[6]Present address: BGI Research, Beijing, China.

[7]Present address: School of Chemistry and Material Sciences, University of Shanghai for Science and Technology, Shanghai, China.

[8]These authors contributed equally

[9]Lead contact

* Corresponding author

E-mail: xwang@jiangnan.edu.cn (X.W.); xiaoyun.liu@bjmu.edu.cn (X.L.); ayan8@hku.hk (A.Y.).

Abstract

Phosphate (Pi) scarcity, a pervasive stressor prevalent in bacterial infections and dysbiotic host environments, potently drives antimicrobial resistance (AMR) against cationic antibiotics like polymyxins across diverse bacterial taxa. While established Pi depletion-induced AMR mechanisms often involve membrane phospholipid remodelling, *Enterobacteriaceae* largely lack these pathways, leaving their Pi scarcity-driven AMR mechanism unresolved. Here, we reveal that Pi limitation robustly induces polymyxin resistance in *Enterobacteriaceae* through 4-amino-4-deoxy-L-arabinose (L-Ara4N) modification of the Gram-negative outer membrane component lipid A, reflecting a distinct adaptive strategy. This modification is driven by strong *ugd-arn* operon induction, mediated by the PmrAB two-component system. We discover that Pi depletion triggers cellular Mg^{2+} release, prompting compensatory Fe^{3+} mobilization to the cell envelope that directly activates PmrAB. Crucially, this metal-dependent signaling axis offers a directly targetable mechanism for reversing polymyxin resistance, a significant deviation from the less accessible, PhoBR-regulated phospholipid remodelling strategies in other bacteria. We demonstrate that Mg^{2+} supplementation or Fe^{3+} chelation effectively suppresses PmrAB activation and restores polymyxin susceptibility, thereby establishing a novel, metal-centric paradigm for understanding and pharmacological intervention in stress-induced AMR.

41 # Introduction

42 Within the dynamic and often hostile environment of the host, nutrient scarcity presents a
43 pervasive challenge for invading bacteria, promoting the evolution of survival strategies
44 and shaping pathogen persistence.[1,2] Among the macronutrients essential for bacteria,
45 phosphorus (P) serves as a critical element for life. It is a fundamental component of key
46 biomolecules such as nucleic acids, phospholipids, and ATP, and plays crucial roles in the
47 essential processes of genetic inheritance, energy metabolism, membrane integrity, and
48 signal transduction.[3,4] The primary assimilable form of phosphorus for bacteria is the
49 orthophosphate anion (PO_4^{3-}), commonly known as inorganic phosphate (Pi). However,
50 Pi is typically found at very low concentrations (<4μM) in diverse environments, from
51 oceans (0.1-3μM),[5,6] and soil (0.0105 to 10.5μM, <1μM near plant roots),[7,8] to critically
52 host-associated niches including macrophages,[9] Salmonella-containing vacuoles,[10] and
53 cystic fibrosis sputum.[11] This localized Pi scarcity is a direct consequence of host
54 nutritional immunity and intense microbial competition.[12,13] Evidence for widespread
55 bacterial adaptation to Pi limitation is abundant, with metagenomic and
56 metatranscriptomic studies consistently revealing robust transcriptional upregulation of
57 high-affinity phosphate acquisition (Pho) regulon genes across various chronic infections
58 and dysbiosis conditions.[11,14,15] Bacteria cope with these pervasive conditions via the
59 conserved PhoBR two-component system, which activates genes for Pi acquisition,
60 transport, and storage when extracellular Pi falls below 4 μM.[3,16,17]

Beyond direct Pi assimilation, Pi depletion triggers broader adaptive responses crucial for pathogen survival, including enhanced virulence and, critically, antimicrobial resistance (AMR).[18-20] For example, Pi limitation upregulates virulence factors in *Vibrio cholerae*, EHEC, and *Pseudomonas aeruginosa*, and conversely, Pi supplementation can reduce infection severity.[21-24] More importantly, Pi depletion is increasingly recognized as a potent environmental cue driving AMR across diverse bacterial taxa, particularly against cationic antibiotics like polymyxins. This is evidenced by increased vancomycin resistance in *Streptomyces coelicolor*,[25] and enhanced polymyxin B/E resistance in *Pseudomonas fluorescens*, *P. aeruginosa*, and *Acinetobacter baumannii* under Pi-limited conditions.[11,26-28] Given that Pi limitation is a prevalent and dynamic stressor in host niches, understanding its role in promoting AMR is vital for developing effective counter-strategies.

Mechanistically, Pi depletion-induced AMR is often linked to the remodelling of bacterial membranes, where phosphorus-containing phospholipids are substituted with diverse non-phosphorous lipids. This strategy spares intracellular phosphate and often modifies membrane charge, which is critical for resistance to cationic antimicrobials. Examples include the accumulation of ornithine lipids (OLs) in *Vibrio cholerae,*[29] diacylglyceryl-N,N,N-trimethylhomoserine (DGTS) in *Rhizobium meliloti*,[30] and *Cryptococcus neoformans*,[31] glycolipids in *Agrobacterium tumefaciens*,[32] and extensive lipidome remodelling in *Mycobacterium tuberculosis*.[33] Specifically for polymyxin resistance, *P. aeruginosa* synthesizes neutral monoglucosyl diacylglycerol (MGDG) and glucuronic acid diacylglycerol (GADG),[11] while *A. baumannii* produces positively charged ornithine- and

lysine-containing aminolipids (OL and LL) under Pi limitation.[27] These diverse lipid modifications effectively reduce the net negative charge of the bacterial membrane, decreasing polymyxin binding and improving resistance.

However, these established lipid-remodelling strategies are not universally conserved. Critically, genes for OL biosynthesis are absent in most *Enterobacteriaceae*, a family of paramount clinical importance, and MGDG/GADG synthesis is not a predominant mechanism for polymyxin resistance in this group.[34-36] Given the widespread prevalence of Pi limitation in host environments and the escalating threat of polymyxin resistance in *Enterobacteriaceae*, a fundamental question with significant clinical implications arises: what alternative, yet unidentified, mechanisms underpin Pi depletion-induced polymyxin resistance in this critical bacterial family, especially in the absence of the established OL and MGDG/GADG pathways?

In this study, we address this critical gap by reporting that Pi limitation also induces polymyxin resistance in *Enterobacteriaceae*, but through a distinct mechanism. Using *E. coli* K-12 MG1655 as a model, we demonstrate that this process involves the upregulation of conserved Ugd and ArnBCADTEF proteins, which catalyse the addition of the positively charged 4-amino-4-deoxy-L-arabinose (L-Ara4N) to lipid A. This adaptive lipid A modification is driven by a novel Pi-Mg-Fe-PmrAB regulatory circuit: loss of membrane-stabilizing magnesium (Mg^{2+}) and compensatory iron (Fe^{3+}) mobilization to the cell membrane activate the PmrAB two-component system, leading to upregulation of the *ugd-arn* operon. Crucially, interfering with this circuit, via Mg^{2+} supplementation or iron

103 chelation, effectively reverses resistance in representative *Enterobacteriaceae* species,
104 but not in non-enteric species like *P. aeruginosa*. Phylogenetic analyses further reveal
105 distinct clades for *E. coli* PmrB (EcoPmrB) and *P. aeruginosa* PmrB (PaePmrB), with
106 PaePmrB lacking the conserved "ExxE" motif required for Fe^{3+} sensing. Our findings
107 uncover a conserved, targetable stress-responsive circuit underlying Pi depletion-induced
108 polymyxin resistance within *Enterobacteriaceae*, offering new avenues for managing
109 stress-induced antibiotic resistance.

110 Results

111 Pi depletion induces polymyxin resistance in *Enterobacteriaceae*

112 To investigate whether Pi limitation induces antibiotic resistance in *Enterobacteriaceae*,
113 we assessed the susceptibility of two representative species, *E. coli* MG1655 and
114 *Salmonella enterica* serovar Typhimurium ATCC14028. Bacteria were initially cultured in
115 standard MOPS synthetic minimal medium containing replete Pi (1.32 mM). Subsequently,
116 cultures were transferred to either Pi-replete (Pi+, 1.32 mM) or acute Pi-depleted (Pi-, 0
117 mM) conditions for 3 hours, a protocol adapted from R G Groat et. al.[37] Following this,
118 bacterial survival was determined via 3-hour polymyxin B killing assays (Figure S1).
119 Polymyxin B concentrations for these assays were established based on the minimum
120 inhibitory concentrations (MICs) of strains in MOPS minimal medium (Table S1) and a
121 preliminary dose-dependent killing assay (Figure S2). Results showed that Pi depletion
122 enhanced the survival of both species against polymyxin B (Figure 1A). Similar Pi

123 depletion-induced polymyxin resistance was also observed in *E. coli* O157 and four
124 uropathogenic *E. coli* strains isolated from urinary tract infection patients in the Queen
125 Mary Hospital, Hong Kong (Figure 1B). Consistent with previous reports, *P. aeruginosa*
126 PAO1 subjected to Pi depletion also display enhanced resistance against polymyxin B
127 (Figure 1B). These results suggest that Pi depletion-induced polymyxin resistance is a
128 widespread phenomenon among Gram-negative bacteria.

129 Pi depletion induces 4-amino-4-deoxy-L-arabinose (L-Ara-4N) 130 modification of lipid A in *Enterobacteriaceae*

131 Since these species lack the MGDG/GADG and OL pathways described in *P. aeruginosa*
132 and *A. baumannii*, we employed *E. coli* K-12 MG1655 as a model to comprehensively
133 investigate the regulatory mechanisms underlying this stress-induced polymyxin
134 resistance. We performed quantitative proteomic analysis on *E. coli* MG1655 cells
135 subjected to the identical growth and treatment conditions as for the polymyxin B
136 challenging assay (Figure S1). Among the 2990 proteins detected which cover 69% of
137 the 4358 proteins annotated in the UniProt *E. coli* MG1655 database, abundance of 225
138 proteins was found to be altered following acute Pi depletion, with 142 proteins
139 upregulated and 83 downregulated (Figure S3) (Table S2). In addition to proteins
140 belonging to the Pho regulon, such as PhoB, PstB, PhoU, and PhnB (Figure 2A) in the
141 COG functional group of transportation and metabolism of inorganic ions (13% of
142 upregulated proteins) (Figure S3), the most abundant functional groups among the
143 significantly upregulated proteins include those involved in cell wall/membrane/envelope

144 biogenesis (13%) and energy production and conversion (10%) (Figure S3). Conversely,
145 proteins involved in translation, ribosomal structure and biogenesis (33%) and amino acid
146 transport and metabolism (17%) were significantly downregulated (Figure S3).

147 Specifically, among the most upregulated proteins ($log_2FC>10$) induced by Pi depletion
148 (Table S2), two proteins encoded in the *arnBCADTEF* operon: ArnB and ArnC, were
149 identified (Figures 2A and 2B). Additionally, two other proteins in the Arn pathway, ArnA
150 and Ugd, were also up-regulated with more than five-fold in response to Pi depletion
151 treatment (Figures 2A and 2B). This finding is particularly intriguing, because Ugd and
152 Arn proteins are known to catalyze the biosynthesis of 4-amino-4-deoxy-L-arabinose (L-
153 Ara4N) and its modification of lipid A (Figure 2B), which confers resistance to the cationic
154 antibiotic polymyxins due to simultaneous neutralization of a negative charge and
155 introduction of a positive charge to lipid A.[38] To verify the upregulation of these proteins,
156 we first examined the mRNA level of *ugd* and *arnB* genes by RT-qPCR and found their
157 levels were 16- and 27-fold higher, respectively, under Pi- than under Pi+ conditions
158 (Figure 2C). Next, we constructed ArnB-3×FLAG in MG1655 chromosome and observed
159 a significant production of the ArnB protein under Pi- conditions, while its level was
160 undetectable under Pi+ conditions (Figure 2D). We also constructed promoter-*lacZ*
161 fusions and observed more than 10-fold higher promoter activities for both *ugd* and *arn*
162 genes under Pi- conditions than Pi+ conditions (Figure 2E), confirming the upregulation
163 of the Ugd-Arn system under Pi depletion.

164 We then extracted lipid A molecules from *E. coli* MG1655 cells cultured under identical

165 conditions as in the proteomic analysis, and analyzed the extract using ESI-MS. Native
166 lipid A, a hexacetylated glucosamine disaccharide with two phosphate groups at position
167 1 and 4' (m/z 1796.98), was detected in *E. coli* cells cultured under Pi sufficient conditions
168 (Figure 2F). In constant, the predominant lipid A species in *E. coli* cells subjected to Pi
169 depletion were found to be modified with L-Ara4N (m/z 1928.67) (Figure 2F). Next, we
170 deleted *arnT*, *arnB*, and *ugd* and found that deletion of these genes abolished Pi
171 depletion-induced polymyxin B resistance in *E. coli* (Figure 2G).

172 The induction of L-Ara4N modified lipid A, along with decrease in the unmodified form,
173 was also observed in *E. coli* O157 (Figure S4A), a representative UTI strain UTI-3 (Figure
174 S4B), and *S.* Typhimurium ATCC14028 (Figure S4C), each exhibiting varying ratios.
175 These fundings indicate that L-Ara4N modification of lipid A is widespread in
176 *Enterobacteriaceae* and correlates with increased polymyxin B resistance. We also
177 analyzed lipid A species in *P. aeruginosa* PAO1 and found that instead of the L-Ara4N
178 modification, a 2-hydroxymyristate modification of lipid A, which is catalyzed by the
179 aspartyl beta-hydroxylase LpxO, was detected in Pi-depletion treated cells (Figure S4D).
180 Altogether, these results indicated that unlike the strategy observed in PAO1 where Pi
181 stress induces resistance by replacing the negatively charged phospholipids with
182 MGDG/GADG, in *E. coli*, resistance is mediated by lipid A modification with L-Ara4N
183 catalyzed by Ugd and Arn proteins.

184 To delineate the sensitivity of the Ugd-Arn pathway to varying Pi levels, we measured the
185 promoter activities of P_{ugd}-*lacZ* and P_{arn}-*lacZ* across a gradient of phosphate

concentrations. We observed that the activities of both P_{ugd}-*lacZ* and P_{arn}-*lacZ* remained robustly activated, at levels comparable to complete Pi depletion (0 mM), even when 0.040 mM or 0.132 mM Pi was supplemented to the medium (Figure S5). When Pi supplementation reached 0.4 mM, their upregulation was attenuated by 60%. These findings collectively suggest that moderate Pi limitation (below 0.4mM) is effective in sustaining the activation of *ugd-arn* genes (Figure S5).

The PmrAB two component system is activated to up-regulate the *arn* operon during Pi depletion

To elucidate the regulatory mechanisms underlying *ugd-arn* upregulation during Pi limitation, we first investigated the involvement of the global phosphate regulators PhoB and PhoR. We found that deleting either PhoB or PhoR did not affect the enhanced polymyxin B resistance or the upregulation of the *arn* operon observed in Pi-depleted *E. coli* (Figures 3A and S6). This observation suggested that other regulatory systems were primarily responsible for upregulating the *arn* gene expression under Pi depletion.

The *arn* operon and *ugd* are known targets of the PmrAB two-component system (TCS) in *E. coli.* [39] (Note the *E. coli* homolog of this system is BasSR; we adopt the PmrAB nomenclature in this study to reflect its direct role in polymyxin resistance and its wider usage in the literature.)[40] To determine if this regulation also extended to Pi depletion, we constructed Δ*pmrB* and Δ*pmrA* mutants. Both the enhanced polymyxin B resistance and the upregulation of the *arn* operon under Pi depletion were abolished in these mutants

206 (Figures 3A and 3B), indicating a critical role for PmrAB in *arn* regulation and polymyxin
207 B resistance during Pi depletion. The promoter activity of *ugd* remained unaffected in
208 Δ*pmrB* and Δ*pmrA* mutants (Figure S7), suggesting a distinct regulatory input for *ugd*.
209 Given that the PhoPQ TCS can indirectly activate the PmrAB regulon in *S*. Typhimurium
210 via PmrD (though this indirect regulation appears absent in *E. coli*), we also examined the
211 contribution of PhoPQ.[41] Deletion of *phoP* or *phoQ* did not alter the enhanced polymyxin
212 B resistance or *arn* operon upregulation under Pi depletion (Figures 3A and S6). These
213 findings suggest that the *arn* system is activated by PmrAB in response to an as-yet-
214 unidentified secondary signal induced by Pi depletion, rather than by direct Pi depletion
215 sensing or through the PhoPQ system.

216 Given the distinct regulation we observed for *ugd* promoter activity, we further investigated
217 its response to the PhoBR system. We measured *ugd* promoter activity in Δ*phoB*, Δ*phoR*,
218 Δ*phoP*, and Δ*phoQ* mutants and found P_{ugd}-*lacZ* activity decreased by approximately 30%
219 in both Δ*phoB* and Δ*phoR* mutants, but not in Δ*phoP* and Δ*phoQ* mutants (Figure S7).
220 This indicates that *ugd* is regulated by the PhoBR system, potentially alongside other
221 pathways, during Pi depletion.

222 Given the central role of the PmrAB system in mediating Pi depletion-induced polymyxin
223 resistance, we next investigated whether *eptA*, another PmrAB-regulated gene,
224 contributes to this phenotype. We constructed a Δ*eptA* mutant and assessed bacterial
225 survival in a polymyxin B killing assay. Deletion of *eptA* had no impact on the enhanced
226 polymyxin B resistance (Figure S8), indicating that *eptA* is not required for the resistance

227 phenotype induced by Pi depletion. This observation was further supported by ESI-MS
228 analysis (Figure 2F), which did not detect phosphoethanolamine (pEtN) modification of
229 lipid A, a hallmark of EptA activity, in Pi-depleted cells. Collectively, these results strongly
230 suggest that the activation of the Arn system via PmrAB is the primary mechanism
231 responsible for Pi depletion-induced polymyxin resistance.

232 To assess whether PmrAB activation occurs under Pi depletion, we examined the
233 phosphorylation status of the response regulator PmrA using Phos-tag SDS-PAGE, which
234 reliably detects phosphorylated PmrA in cells treated with known activator Fe^{3+}.[42] Results
235 showed that phosphorylated PmrA was detected in cells subjected to Pi depletion (Figure
236 3C), demonstrating that PmrAB TCS is indeed activated under Pi depletion condition. To
237 further confirm this in vivo, we performed a FRET-based whole-cell transcription factor-
238 promoter binding assay.[43] We incorporated a bright fluorescent unnatural amino acid, L-
239 (7-hydroxycoumarin-4-yl) ethylglycine (CouA)[44] at position G137 within the DNA-binding
240 domain of PmrA through genetic encoding, allowing it to serve as the FRET donor (Figure
241 3D).[43] The nucleic acid dye SYTO9 was utilized to stain promoter DNA of PmrA regulon
242 (Figure 3D),[43] acting as the FRET acceptor. The whole-cell FRET assay revealed that,
243 similar to the treatment with excessive $FeSO_4$ (500μM),[43] a FRET signal indicative of
244 PmrA binding to its target promoters was observed in cells subjected to Pi depletion
245 without excessive $FeSO_4$ (Figure 3E). These results confirmed that Pi depletion induced
246 activation of the PmrAB signal transduction system in *E. coli.*

Pi depletion drives Fe^{3+} elevation in *E. coli* cells to activate the PmrAB TCS

PmrAB has been previously reported to be activated by ferric ion (Fe^{3+}), zinc ions (Zn^{2+}), aluminum ions (Al^{3+}), or acidic pH.[45,46] Since no Al^{3+} was added in the culture, and the pH remained largely unchanged (7.2-7.0) across the Pi depletion treatments (Figure S9), we focused on the two metal ions and examined cellular metal profiles including iron (Fe), zinc (Zn), magnesium (Mg), copper (Cu), and calcium (Ca). ICP-MS analysis revealed a significant, greater than 5-fold increase in cellular Fe content under Pi depletion, compared to Pi-sufficient conditions (Figure 4A). Conversely, cellular Mg levels decreased, while Cu, Zn, and Ca levels remained largely unchanged (Figure 4A). Corroborating this cellular Fe accumulation, the Fe content in the spent medium decreased after 3 hours of *E. coli* incubation under Pi depletion (Figure 4B), indicating active Fe mobilization from the medium into *E. coli* cells. These findings strongly implicated Fe^{3+} as the activating signal for PmrAB under Pi depletion.

Given that *S.* Typhimurium PmrB (StPmrB) senses Fe^{3+} through conserved glutamic acid residues (E36, E39, E61, E64) in its periplasmic domain,[42] we hypothesized a similar mechanism for *E. coli* PmrB (EcoPmrB). To test this, we generated chromosomal *pmrB*E36A and *pmrB*E39A mutations in *E. coli* MG1655 (Figure 4C). Consistent with their proposed role in Fe^{3+} sensing, these mutations abolished the P*arn-lacZ* reporter response to exogenous Fe^{3+} (100 μM) (Figure S10). Crucially, both mutations also abolished *arn* operon upregulation under Pi depletion (Figure 4D), demonstrating that Pi depletion-

268 induced PmrAB activation requires the Fe^{3+} sensing capability EcoPmrB.

269 To confirm the necessity of Fe mobilization, we observed that *arn* operon upregulation
270 was abolished when cells were grown in Fe-free, Pi-depleted medium (Figure 4E).
271 Although Pi depletion significantly impaired bacterial growth (doubling time increased
272 from ~1 hr to ~6 hrs), co-depletion of Fe did not further exacerbate this effect, confirming
273 that the observed PmrAB activation specifically responds to Pi-related Fe mobilization
274 rather than general growth inhibition (data not shown). Investigating the sensitivity of this
275 response, we found that reintroduction of Fe to Pi-depleted cells restored P*arn-lacZ*
276 activity in a dose-dependent manner (Figure 4F), further confirming the role Fe
277 mobilization in activating PmrAB and *arn* genes during Pi depletion. Importantly, *arn*
278 activation in Pi-starved cells occurs at significantly lower exogenous Fe concentrations
279 (~10-fold less) than in Pi-sufficient conditions (Figure 4F), suggesting an enhanced
280 cellular capacity for Fe mobilization or sensing under Pi depletion.

281 Pi depletion triggers Mg^{2+} loss, leading to Fe^{3+} mobilization to
282 membrane and PmrAB activation

283 To elucidate the mechanism of Fe mobilization during Pi depletion, we first investigated
284 the role of canonical iron uptake pathways. Surprisingly, deletion of genes encoding outer
285 membrane iron-chelator complex receptors and enterobactin synthetase (*fecA*, *fepA*, *fiu*,
286 *cirA*, *entE*), individually or as a penta-deletion mutant (Δ5Fe), did not abolish P*arn-lacZ*
287 induction during Pi depletion (Figure S11A). ICP-MS analysis further confirmed that cell-

288 associated Fe still increased by over 5-fold in Δ5Fe cells during Pi depletion (Figure S11B).
289 These results indicated that Fe-mediated PmrAB activation during Pi depletion was
290 independent of enhanced intracellular Fe uptake and suggested an alternative
291 mechanism, likely involving Fe association with the cell surface, consistent with the known
292 ability of PmrAB to sense periplasmic and surface-bound Fe^{3+}.[42]

293 The outer leaflet of the Gram-negative outer membrane (OM) primarily consists of lipid A,
294 whose negatively charged phosphate groups are typically neutralized by cell-associated
295 Mg^{2+} and Ca^{2+} to maintain membrane stability.[47] Our ICP-MS analysis revealed a 44%
296 reduction in cellular Mg content, while Ca^{2+} levels remained unchanged, in *E. coli* cells
297 following 3 hours of Pi depletion treatment (Figure 4A). Monitoring the dynamics revealed
298 that cellular Mg progressively decreased upon transferring *E. coli* cells to Pi-depleted
299 medium, continuing over a 5-hour period (Figure 5A). This Mg^{2+} loss was independent of
300 Fe, as a similar degree of loss occurred in Fe-free, Pi-depleted medium (Figure S12).
301 Conversely, cellular Fe increased, peaking after two hours of Pi depletion before slightly
302 declining (Figure 5A). The temporal correlation between Fe accumulation and P*arn-lacZ*
303 activity (Figure 5B) suggested active Fe mobilization to the cell surface during Pi depletion,
304 potentially to compensate for Mg^{2+} loss and stabilize the membrane. The subsequent
305 activation of the PmrAB-Arn system that remodel lipid A by decreasing negative charges,
306 might thus represent an adaptive response to physiological changes, such as OM
307 instability, caused by Mg^{2+} dissociation. Supporting this, deletion of *pmrA* led to an even
308 greater and sustained increase in Fe mobilization during Pi depletion (Figure 5C), which

309 could be toxic to *E. coli*.[42]

310 To directly assess Fe association with the cell surface, we washed cell pellets with
311 deferoxamine (DFOM)-containing buffer, a membrane-impermeable Fe^{3+}-specific
312 chelator.[48] ICP-MS analysis showed that washing with DFOM-supplemented buffer
313 significantly reduced Fe content in cells treated with Pi depletion but had no significant
314 effect on cells harvested from Pi-sufficient conditions (Figure 5D). Quantification revealed
315 that Pi-starved cells exhibited a two-fold greater loss of Fe upon DFOM washing
316 compared to Pi-sufficient conditions (Figure 5E), demonstrating that Pi depletion
317 promoted Fe mobilization to cell surfaces, where it remained susceptible to removal by a
318 membrane-impermeable chelator.

319 To uncover the driving force behind this enhanced Fe mobilization, we supplemented the
320 culture medium with excess Mg (10 mM) to counteract Mg loss. This supplementation
321 significantly reduced Fe mobilization to MG1655 cells during Pi depletion (Figure 6A);
322 correspondingly, P_{arn}-*lacZ* activity declined as Mg concentration increased in the Pi-
323 depleted medium (Figure 6B). These results strongly suggest that Fe mobilization to the
324 cell surface during Pi depletion is dependent on Mg^{2+} loss. Further, monitoring Mg^{2+}
325 dynamics in the spent medium revealed a continuous increase in Mg levels throughout
326 the Pi depletion treatment (Figure 6C), confirming active Mg^{2+} dissociation from the cells.
327 Similar Mg^{2+} release was observed even during combined Mg and Pi depletion (Figure
328 S13). These results suggested that while Mg^{2+} is essential for bacterial growth, an
329 imbalance with phosphorus during Pi depletion appears to trigger active Mg^{2+} dissociation

330 from the cells. A comparable 45% Mg^{2+} loss was also observed in *P. aeruginosa* PAO1
331 under similar conditions (Figure S14). However, Fe mobilization was less pronounced
332 (2.4-fold vs. 5.4-fold in *E. coli*), reflecting species-specific adaptation strategies.[11]

333 Given that membrane-associated Mg^{2+} primarily neutralizes the negative charges of lipid
334 A to stabilize the OM, we hypothesized that Mg^{2+} loss during Pi depletion alters OM
335 properties, and Fe mobilization may serve to stabilize the OM. To test this, we employed
336 an OM-sensitive probe.[49] The probe reports membrane surface properties through two
337 orthogonal readouts: an overall fluorescence increase, which reflects probe disassembly
338 upon binding to the anionic bacterial surface, and the pyrene excimer-to-monomer
339 emission ratio (I_{482}/I_{375}), which captures differences in local surface interactions. The 2D
340 sensor output revealed distinct signals between cells grown under Pi-sufficient and Pi-
341 depleted conditions (Figure 6D), indicating altered OM characteristics. Notably, cells
342 grown in Fe-free, Pi-depleted medium exhibited even greater shifts (Figure 6D),
343 suggesting that Fe mobilization and subsequent activation of the PmrAB-Arn pathway
344 served as an adaptation strategy to maintain OM integrity during Pi stress. This strategy
345 likely prevents uncontrolled Fe accumulation and toxicity,[42] ultimately resulting in stress-
346 induced polymyxin resistance. A schematic model illustrating this process is presented
347 (Figure 7).

348 Disrupting the Mg-Fe-PmrAB-Arn circuit counters Pi depletion-
349 induced polymyxin resistance in *Enterobacteriaceae*

350 Our findings above identified a Mg-Fe-PmrAB-Arn circuit underpinning the polymyxin
351 resistance induced by stress adaptation to Pi depletion. To evaluate whether interference
352 with this pathway could mitigate the stress-induced polymyxin resistance, we
353 supplemented Pi depletion medium with excess Mg^{2+} (10mM) or applied a membrane
354 impermeable chelator DFOM (10μM). Both approaches effectively suppressed Pi
355 depletion-induced polymyxin resistance in *E. coli* and *S.* Typhimurium (Figure 8A). In
356 contrast, neither intervention reversed polymyxin resistance in *P. aeruginosa* despite
357 various combinations of Mg^{2+} supplementation and Fe chelation (Figure S15). This
358 highlights species-specific adaptative strategies and aligns with several observations
359 from our study as well as several previous research.[11,50] Specifically, in *P. aeruginosa,*
360 despite a 45% Mg loss during Pi depletion, Fe levels increased only two-fold compared
361 to over five-fold in *E. coli*, consistent with its reliance on MGDG/GADG lipids synthesis
362 regulated by the PhoBR system (Figure 8B).[11] Additionally, *P. aeruginosa* exhibits a
363 distinct lipid A modification, 2-hydroxy myristate (Figure S4D), that does not confer
364 polymyxin resistance.[51] Phylogenetic analysis of 250 PmrB homologs revealed that
365 EcoPmrB and PaePmrB cluster in separate clades, with PaePmrB lacking the conserved
366 "ExxE" motif essential for Fe^{3+} sensing (Figure 8C). Together, these findings underscore
367 the diverse stress response strategies employed by different classes of Gram-negative
368 bacteria and highlight the importance of understanding species-specific regulatory
369 mechanisms for developing targeted interventions against stress-induced antibiotic
370 resistance.

371 # Discussion

372 Bacterial adaptation to environmental stressors is crucial for survival and pathogenesis.
373 Phosphate (Pi) scarcity, a pervasive condition in diverse environments including host-
374 associated niches such as macrophage phagosomes, salmonella-containing vacuoles,
375 and cystic fibrosis sputum, is a potent cue driving antimicrobial resistance (AMR) against
376 cationic antibiotics such as polymyxins.[9-11] Adaptive mechanisms previously
377 characterized for Pi depletion-induced AMR often involve remodeling bacterial
378 membranes by substituting phosphorus-containing phospholipids with Pi-free, neutral, or
379 positively-charged lipids.[11,26-28] However, the specific mechanisms in clinically important
380 Enterobacteriaceae, which largely lack these canonical phospholipid remodeling
381 pathways, have remained largely unknown. In this study, we unveil a conserved, yet
382 distinct, polymyxin B resistance mechanism in *Enterobacteriaceae*: Pi limitation triggers a
383 cascade of cationic imbalance and Fe^{3+} signaling, leading to L-Ara4N modification of lipid
384 A and outer membrane remodeling, a process distinct from phospholipid-based resistance
385 pathways (Figure 7). This intricate Mg-Fe-PmrAB regulatory circuit represents a
386 previously unappreciated ecophysiological vulnerability, offering a novel strategy to
387 mitigate stress-induced polymyxin resistance.

388 Maintaining a balanced P/Mg ratio is paramount for bacterial cellular physiology, with ATP
389 and rRNA serving as primary cytoplasmic reservoirs for both Pi and Mg^{2+}.[52-55] Previous
390 work by Bruna et al. demonstrated that bacteria suppress Pi uptake under Mg^{2+} limitation

391 to preserve cellular function.[53] Herein, our study extends this understanding by showing
392 that Pi scarcity itself actively triggers Mg^{2+} release from *E. coli* cells. This observation
393 underscores the tightly coupled nature of Pi and Mg^{2+} homeostasis. Our comprehensive
394 proteomic analysis further supports this, revealing that proteins involved in translation,
395 ribosomal structure, and biogenesis were among the most significantly downregulated
396 groups during Pi depletion (Figures 1A and S3). Concurrently, we observed a steady
397 decline in cellular ATP levels under Pi-limited conditions (Figure S16), suggesting a
398 profound arrest in ribosome biogenesis and protein synthesis that likely contributes to the
399 observed Mg^{2+} release and cellular loss.

400 In *Enterobacteriaceae*, Mg^{2+} homeostasis is primarily governed by the PhoPQ two-
401 component system, which is well-characterized in *S.* Typhimurium to be activated under
402 low extracellular Mg^{2+} conditions.[56,57] Given the observed Mg^{2+} release during Pi-depletion,
403 we investigated the involvement of this classical Mg^{2+}-sensing PhoPQ system. Our results
404 showed that despite cellular Mg^{2+} loss during Pi depletion, the transcription of key PhoPQ
405 regulon genes, such as *phoQ* and *mgtA*, remained unchanged (Figure S17). This
406 indicates that while cellular Mg^{2+} levels are perturbed, they do not drop sufficiently to
407 activate the canonical PhoPQ response. Instead, our data compellingly demonstrate that
408 under acute Pi depletion, *Enterobacteriaceae* preferentially engage an alternative, Fe^{3+}-
409 mediated membrane remodeling pathway. This pathway activates the *arn* operon and
410 subsequent L-Ara4N modification independently of the classical Mg^{2+}-sensing PhoPQ
411 system, highlighting a distinct adaptive strategy.

412 This Fe^{3+}-mediated lipid A modification strategy in *Enterobacteriaceae* offers a stark
413 contrast to Pi depletion-induced polymyxin resistance mechanisms described in other
414 Gram-negative bacteria, notably *P. aeruginosa*. In *P. aeruginosa*, Pi depletion primarily
415 activates the PhoBR regulon, orchestrating the biosynthesis of phosphorus-free
416 glycolipids (MGDG and GADG) to replace negatively charged phospholipids and maintain
417 membrane integrity (Figure 8B).[11] While *P. aeruginosa* possesses a PmrAB homolog, its
418 PmrB sensor kinase lacks the critical Fe^{3+}-sensing "ExxE" motifs found in
419 *Enterobacteriaceae* PmrB, precluding direct Fe^{3+} response. Instead, PmrAB activation in
420 *P. aeruginosa* is typically coupled to the PhoPQ system, which senses low extracellular
421 Mg^{2+}. Thus, while *P. aeruginosa* employs PhoBR-regulated phospholipid remodeling as
422 its primary Pi depletion response, *Enterobacteriaceae*, largely lacking these glycolipid
423 pathways, have evolved to utilize a secondary, Fe^{3+}-sensing mechanism. Here, the
424 PmrAB system, via its specific Fe^{3+}-sensing "ExxE" motifs in PmrB, orchestrates
425 membrane remodeling through L-Ara4N modification of lipid A as a key physiological
426 adaptation to Pi depletion.[50] While *P. aeruginosa* also exhibits lipid A modification (e.g.,
427 2-hydroxymyristate by LpxO) during Pi depletion, this modification does not contribute to
428 polymyxin resistance and is regulated independently of PhoBR, PhoPQ, or PmrAB,
429 highlighting distinct physiological roles.[51]

430 The biosynthesis of L-Ara4N and its transfer to lipid A are mediated by Ugd and
431 ArnABCDEFT proteins, encoded by the *ugd* gene and the *arn* operon, respectively[58-61].
432 Our data reveal a sophisticated regulatory separation: during Pi depletion, *arn*

433 transcription is tightly controlled by the PmrAB system, while ugd expression is not
434 PmrAB-dependent and exhibits partial regulation by the PhoBR system (Figure S6). This
435 bifunctional control is not unexpected, as *ugd* encodes UDP-glucose dehydrogenase, an
436 enzyme with dual roles in L-Ara4N biosynthesis and in the production of
437 exopolysaccharides like colanic acid.[62,63] Therefore, while PmrAB activation of *arn* is
438 absolutely critical for L-Ara4N modification of lipid A during Pi limitation, *ugd* regulation
439 reflects its broader involvement in diverse cellular metabolic and stress responses.

440 While preparing this manuscript, a recent study by Baijal et al. (2024) reported that the
441 *ppk* gene modulates *arn* operon upregulation under combined nutrient limitations (transfer
442 from rich LB to low-Pi, no-amino-acid MOPS medium) in *E. coli.*[64] Inspired by this, we
443 investigated the role of *ppk* in polymyxin resistance specifically under Pi depletion, our
444 primary focus. We found that *ppk* deletion did not affect *arn* or *ugd* promoter activity under
445 sole Pi-depleted conditions (Figure S18), indicating its dispensability when Pi is the only
446 limiting factor. To reconcile these findings, we replicated the Baijal et al. experimental
447 conditions, confirming *ppk*-dependent *arn* upregulation under combined Pi and amino acid
448 scarcity (Figure S19A). Our subsequent experiments, systematically disentangling these
449 stresses, revealed that while both Pi and amino acid depletion induce *arn* upregulation, Pi
450 depletion is the dominant driver, and *ppk*-dependent regulation emerges only under
451 combined Pi and amino acid scarcity (Figure S19B). These results clarify that while *ppk*
452 influences *arn* expression under specific multifactorial stresses, our identified PmrAB-arn

453 pathway is independently and dominantly activated by Pi depletion alone, providing
454 precise mechanistic insight into this fundamental environmental stressor.

455 In both natural habitats and host-associated niches, Pi scarcity imposes dual challenges:
456 nutrient acquisition and defense against antimicrobial threats. The Pi-Mg-Fe-PmrAB
457 regulatory circuit we have uncovered likely represents a sophisticated adaptive strategy
458 for *Enterobacteriaceae*, facilitating their survival in highly heterogeneous environments
459 with fluctuating Pi levels, such as during host colonization, transmission, or environmental
460 persistence.[65] This PmrAB-mediated membrane remodeling not only confers resistance
461 to polymyxins but may also enable bacteria to preserve membrane integrity and withstand
462 other cationic antimicrobial peptides (CAMPs) produced by competing microbes or host
463 defenses.

464 In summary, our findings elucidate a conserved yet distinct regulatory circuit in
465 *Enterobacteriaceae* that intricately links Pi and Mg^{2+} homeostasis to Fe^{3+}-mediated lipid
466 A modification, driving stress-induced antibiotic resistance. This mechanism is notably
467 distinct from those characterized in *P. aeruginosa* or *A. baumannii*. Crucially, we
468 demonstrate that targeting this circuit effectively mitigates stress-induced resistance.
469 Given that polymyxins remain indispensable as last-line antibiotics for treating multidrug-
470 resistant Gram-negative bacterial infections, our study not only offers critical insights into
471 the fundamental molecular mechanisms underlying stress-induced resistance but also
472 highlights a promising avenue for informing novel resistance management strategies.

473 # Materials and methods

474 ## Bacterial strains and growth conditions

475 Strains, plasmids, and primers used in this study are listed in the S2 and S3 Tables.
476 Bacteria were cultured in lysogeny broth (LB) broth/plates or MOPS minimal medium.
477 MOPS medium was freshly prepared from 1× MOPS stock by supplementing 0.1 % (w/v)
478 glucose and 1.32 mM K_2HPO_4. Acute Pi depletion was applied by transferring bacteria
479 culture into the non-Pi MOPS medium. 1× MOPS consists of 40 mM MOPS, 4 mM Tricine,
480 10 μM $FeSO_4 \cdot 7H_2O$, 9.5 mM NH_4Cl, 0.276 mM K_2SO_4, 0.5 μM $CaCl_2 \cdot 2H_2O$, 525 μM $MgCl_2$,
481 50 mM NaCl, 0.003 μM $(NH_4)_6Mo_7O_{24}$, 0.4 μM H_3BO_3, 0.03 μM $CoCl_2$, 0.01 μM $CuSO_4$,
482 0.08 μM $MnCl_2$, and 0.01 μM $ZnSO_4$. Antibiotics applied to select and maintain the
483 construct were chloramphenicol (25 μg/ml), kanamycin (20 μg/ml) and ampicillin
484 (100 μg/ml).

485 ## Lipid A extraction and ESI-MS analysis

486 Lipid A was extracted from designated *E. coli* cells using Bligh-Dyer method as described
487 with minor modifications.[66] *E. coli* MG1655 cultured in MOPS medium to OD_{600} of 0.5 was
488 harvested as cells under Pi sufficient condition. The same volume of cells was washed
489 with Pi depletion medium for 3 times and resuspended in Pi depletion medium and shake
490 for 3 hrs at 37°C as cells subjected to Pi depletion. 200 ml of each type of cell pellets with
491 three biological replicates were harvested by centrifugation at 4500 rpm for 30 min and

492 washed with H_2O. The cell pellets were suspended in 76 ml of a single-phase Bligh-Dyer
493 mixture (chloroform: methanol: water=1:2:0.8; v/v/v) and stirred at room temperature for
494 1 h. Insoluble debris was collected by centrifugation at 4500 rpm for 30 min, washed with
495 60 ml single-phase Bligh-Dyer mixture, and suspended in 27 ml of 12.5 mM sodium
496 acetate (pH 4.5). The mixture was heated at 100°C for 30 min and cooled to room
497 temperature. The suspension was mixed with 30 ml chloroform and 30 ml methanol.
498 Following vigorously shaken for extraction of lipid A and centrifugation for 30 min, the
499 lower phase containing lipid A was collected and dried with a rotary evaporator.

500 All the mass spectra of lipid A samples were acquired using Waters SYNAPT quadrupole
501 time-of-flight mass spectrometer (MS) equipped with an electrospray ionization source[67].
502 Lipid A samples were dissolved in a mixture of chloroform and methanol (4 : 1; v/v) and
503 subjected to ESI/MS in the negative ion mode. Data acquisition and analysis were
504 performed using MASS LYNX V4.1 software, Waters, Milford, MA, USA.

505 ICP-MS and DFOM treatment

506 Total cellular metal content was quantified using inductively coupled plasma mass
507 spectrometry (ICP-MS) following previous description with minor modifications[68]. *E. coli*
508 cells equivalent to OD_{600} as 5 were harvested by centrifugation at 4500 rpm for 15 mins
509 and washed three times with ice-cold PBS buffer. Cell pellets were subjected to acid
510 digestion with 100 µl 65.0 % HNO_3 (Fluka) at 65°C for 16hrs. Samples were diluted to a
511 final volume of 15 ml with 1% HNO_3 and subjected to ICP-MS detection on Agilent 7900

512 system (Agilent Technologies, CA). Samples were further diluted if the signals exceeded
513 the liner range of standard curve. The standard curves of tested metals were generated
514 from multi-element calibration standard-2A for ICP-MS (Agilent). Metal contents in
515 bacteria were calculated based on the standard curve and results were normalized to
516 original cell number.

517 Deferoxamine mesylate salt (sigma) were applied to examine the degree of iron
518 association to *E. coli* cell surface. *E. coli* cells equivalent to OD_{600} as 5 were harvested by
519 centrifugation at 4500 rpm for 15 mins. Cell pellets were resuspended in HEPES buffered
520 saline with and without 50μM DFOM and incubated in 37°C for 30 mins with 220rpm
521 agitation. Total cellular metal content of these treated cells was quantified using
522 inductively coupled plasma mass spectrometry (ICP-MS) as described above.

523 OM feature monitoring using PI-BactD

524 OM feature of *E. coli* was monitored by an OM-sensitive probe PI-BactD following previous
525 description with minor modifications.[49] *E. coli* cells grown under designated conditions
526 were harvested by centrifugation at 13000 rpm for 2 mins and washed with PBS buffer
527 (10 mM, pH 7.2) twice. Cell pellets were resuspended in PBS buffer to an OD_{600} of 0.5.
528 Fluorescence probe PI-BactD (gift from prof. Xu Z, Dalian) was added into 1mL cell
529 suspension to a final concentration of 2 mM and incubated at room temperature for 1 min.
530 Output signals of two channels: fluorescence increase ($\Delta S/S_0$) and fluorescence ratio
531 metric changes (I_{482}/I_{375}) were recorded to plot the 2D graph (Thermo Scientific

532 Varioskan® Flash spectral scanning multimode reader). Six replicates were conducted for
533 each strain and treatment.

534 Construction of $P_{promoter}$-*lacZ* (P_{arn}-*lacZ* as example) fusion in the
535 single-copy plasmid pNN387

536 A DNA fragment corresponding to the -200 to -1 region relative to the ATG start codon of
537 *arnB* was amplified using *E. coli* MG1655 genomic DNA as the template and primers
538 specific to this fragment flanked with NotI and HindIII restriction sites at the 5'- and 3'-end,
539 respectively. Following digestion with NotI and HindIII and purification using the MiniBEST
540 agarose gel DNA extraction kit (TaKaRa), the fragment was ligated into the plasmid
541 pNN387 which was treated with the same restriction enzymes using the quick ligation kit
542 (NEB). The resulting construct was selected on LB agar plates supplemented with
543 chloramphenicol (25 μg/ml) and was verified by DNA sequencing (BGI, Shenzhen).

544 Beta-galactosidase activity assay

545 β-gal activity assay was performed based on a previous description with modifications.[68]
546 Cells were grown under designated conditions until OD_{600} reached 0.4. 10 μg/ml
547 tetracycline was added to stop cell growth and protein synthesis, and cells were left on
548 ice until being assayed. 100μl of cell culture and 400 μl of Z buffer (60 mM Na_2HPO_4, 40
549 mM NaH_2PO_4, 10 mM KCl, 1 mM $MgCl_2$, 50 mM β-mercaptoethanol, pH 7.0, 4 °C) were
550 mixed. One drop of 0.1% SDS and two drops of chloroform were added to lyse the cells.
551 The reactions were initiated by adding 100 μl of 4 mg/ml ortho-nitrophenyl-β-galactoside

552 into cell suspension and were incubated at 28 °C. Color development in the mixtures was
553 monitored. Finally, 250μl of 1M Na_2CO_3 was added to stop the reaction. Color of the
554 mixtures were measured using spectrophotometer at OD_{420} and OD_{550}. The expression
555 value in Miller units was calculated, and results are presented as the mean of three
556 biological replicates.

557 RNA extraction and RT-qPCR

558 Bacterial cells grown under designated conditions was subjected to RNA extraction when
559 the OD_{600} reached 0.4. Cells were harvested by centrifugation at 4,500 rpm for 10 min at
560 4 °C. After removing the supernatant, the cell pellet was stored at -80 °C to aid cell lysis.
561 Total RNA was extracted using the MiniBEST Universal RNA Extraction Kit (Takara,
562 Japan) according to the manufacturer's instruction. Reverse transcription (RT) was
563 performed using PrimeScript™ RT reagent Kit (Takara, Japan). Quantitative PCR was
564 performed using specific primers and the TB Green® Premix Ex Taq™ (Takara, Japan)
565 in a 20 μL reaction system. The reaction was performed in the ABI StepOnePlus real time
566 PCR system with *rrsB* as reference gene to normalize the relative expression of the target
567 genes. The results were presented as fold change expression of the target genes, and
568 results were presented as the mean of three biological isolates.

569 Construction of clean gene deletion, point mutation and tag insertion
570 in chromosome of *E. coli* MG1655

571 Gene deletion, mutation, and tag insertion in chromosomal were achieved employing a
572 CRISPR/Cas9-mediated approach developed by Zhao et al. with modifications.[69] For
573 gene deletion (deletion of *lacZ* as example), *E. coli* MG1655 was electrotransformated
574 with pCAGO plasmid which contains both SpCas9 and λ-RED to obtain MG1655-pCAGO.
575 A single colony of the resulting transformant was inoculated into LB medium
576 supplemented with ampicillin (100 mg/ml) and grew overnight at 30°C. 100 μl of the
577 overnight culture was inoculated into 10 ml fresh culture medium and cells were grown at
578 30°C with IPTG (0.1 mM) induction to OD600 as 0.6. The cells were collected and washed
579 with cold ddH_2O for three times, generating competent cells for electroporation. An aliquot
580 comprising 100 μl competent cells was mixed with 800 ng of the editing-cassette which
581 encompasses 40 bp of sequence among the CDS of *lacZ* gene followed by the
582 chloramphenicol resistant gene, the N20PAM sequence
583 (GTCCATCGAACCGAAGTAAGG), 40 bp upstream-homologous arm of *lacZ* gene, and
584 40bp downstream-homologous arm of *lacZ* gene, in a 2 mm Gene Pulser cuvette (Bio-
585 Rad) and was subjected to electroporation at 2.3 kV. Following recovering the
586 transformants by cultivation in LB medium for 2 hrs at 30°C, the mixture was spread onto
587 LB agar plate supplemented with ampicillin (100mg/ml), chloramphenicol (25 mg/ml), and
588 1% glucose (to avoid the background expression of the Cas9 protein). Single colonies
589 were collected and verified by colony PCR to obtain an authentic clone in which the
590 editing-cassette was embedded in chromosomal. The confirmed colony was inoculated
591 into LB medium supplemented with ampicillin (100 mg/ml), IPTG (0.1 mM), and L-
592 arabinose (0.2%) at 30°C overnight to enable expression of SpCas9 and the λ-RED

593 recombinase. The cells were then streaked on LB agar plates supplemented with
594 ampicillin (100mg/ml). Following colony PCR, desired colonies containing deletion of the
595 *lacZ* gene were verified by DNA sequencing (BGI, Shenzhen). For point mutation,
596 (mutation of *pmrB* E36 to A as example) *E. coli* MG1655 was conducted following the
597 same procedures except for the editing cassette sequence which encompasses 40 bp of
598 upstream-homologous arm of GAA (Glu36) followed by the chloramphenicol resistant
599 gene, the N20PAM sequence, the 40 bp upstream-homologous arm of GAA (Glu36), GCA
600 (Ala) and 40 bp downstream-homologous arm of GAA (Glu36). For tag insertion, (insertion
601 3xFLAG to C-terminal of *arnB* gene as example) *E. coli* MG1655 was conducted following
602 the same procedures except for the editing cassette sequence which encompasses 40 bp
603 of upstream-homologous arm of stop codon of *arnB* gene followed by the chloramphenicol
604 resistant gene, the N20PAM sequence, the 40 bp upstream-homologous arm of stop
605 codon of *arnB* gene, tag sequence and 40 bp downstream-homologous arm of stop codon
606 of *arnB* gene (include stop codon). After obtaining all desired genome modifications, the
607 editing plasmid was cured by growing the resulting cells at 42°C for 48 hrs.

608 Construction of pET28A-pBAD-*pmrA* for PmrA protein expression

609 A DNA fragment encoding the PmrA protein was amplified using genomic DNA of *E. coli*
610 MG1655 as the template and primers specific to this fragment flanked with NcoI and XhoI
611 restriction sites at the 5'- and 3'-end, respectively. After digestion with NcoI and XhoI, and
612 purification using the MiniBEST agarose gel DNA extraction kit (TaKaRa), the purified
613 fragment was ligated into the plasmid pET28a-pBAD and pET28a-pBAD-3xFLAG [43] which

614 was treated with the same restriction enzymes using the quick ligation kit (NEB). The
615 resulting construct was selected on LB agar plates supplemented with kanamycin (20
616 μg/ml) and was verified by DNA sequencing (BGI, Shenzhen). All plasmids constructed
617 are listed in the supplementary S3 Table.

618 **Immunoblot analysis**

619 Protein levels of ArnB and PmrA were analyzed by SDS-PAGE following Western Blot.
620 1ml of cells with OD_{600} of 0.5 was collected and resuspended in 200 μl sample buffer (13
621 mM Tris, 0.2% SDS, 5% glycerol, 0.004% bromophenol blue, pH 6.8) before being
622 subjected to cell lysis by sonication. Following centrifugation at 13000 rpm for 10 min at
623 4°C, 20 μl of the sample was separated on SDS-PAGE gels (TGX FastCast Acrylamide
624 Kit, 10%, BIO-RAD). Proteins were then transferred onto a polyvinylidene difluoride
625 (PVDF) membrane (BIO-RAD) using a Trans-Blot SD Semi-Dry Transfer Cell (BioRad) at
626 constant voltage (25 V) for 7 min. Membranes were blocked for 1 h with 5% non-fat milk
627 solution in TBST (20 mM Tris, 150 mM NaCl, 0.1% Tween-20) at room temperature
628 followed by incubation with 1:10,000 primary antibody (monoclonal or polyclonal anti-His
629 antibody) in 1% non-fat milk in TBST at room temperature with shaking for 1 hour. After
630 washing with TBST, the membrane was incubated with the secondary antibody (Goat anti-
631 mouse IgG HRP conjugate) in 1% non-fat milk in TBST at room temperature with shaking
632 for 1 hour. Chemiluminescence of protein bands was detected by ECL Plus Western
633 Blotting Detection Reagents (GE Healthcare, USA), and imaged using a X-ray film
634 development by Alliance Q9 (UVITEC, United Kingdom).

635 **Phos-tag SDS-PAGE**

636 In vivo phosphorylation of PmrA was examined using Phos-Tag SDS-PAGE following our
637 previous description with minor modifications.[43] *E. coli* MG1655Δ*pmrA* cell harboring
638 pET28a-pBAD-*pmrA*-3×FLAG (AY7068) was inoculated into MOPS minimum medium
639 supplemented with kanamycin (20 μg/ml) and grew overnight at 37°C. 100 μl of the
640 overnight culture was inoculated into 5 ml fresh MOPS medium and grew at 37°C for 4
641 hrs. Expression of PmrA was induced with 1mM L-arabinose for 1 hr. Cells were collected
642 by centrifugation at 13000 rpm and were washed with MOPS medium supplemented with
643 0.1, 0.5, or 1 mM $FeSO_4$ or Pi- MOPS medium twice and shake for 1 hr at 37°C in the
644 corresponding medium. 1ml of cells with OD_{600} of 0.5 was collected for the subsequent
645 analysis. Cell pellet was washed with cold PBS twice and was resuspended in 200 μl
646 sample buffer (13 mM Tris, 0.2% SDS, 5% glycerol, 0.004% bromophenol blue, pH 6.8)
647 before being subjected to cell lysis by sonication. Following centrifugation at 13000 rpm
648 for 10 min at 4°C, 20 μl of the sample was loaded onto a 10% Tris-Gly polyacrylamide gel
649 containing 25 mM Phos-tag Acrylamide (Wako) and 50 mM $MnCl_2$. Samples were
650 separated by electrophoresis for 2 hrs at 4°C, following washing with 50 ml transfer buffer
651 containing 10 mM EDTA for 20 min to remove residual Mn^{2+}. Proteins on the gel were
652 transferred onto a PVDF membrane. The membrane was blocked with 5% non-fat milk in
653 TBST buffer and was incubated subsequently with monoclonal ANTI-FLAG® M2 antibody
654 (Sigma) and goat anti-mouse IgG (H+L)-HRP conjugate (Bio-rad). To detect FLAG-tagged
655 protein bands, the membrane was submerged in the ECL Plus Western Blotting Detection

656 Reagents (GE Healthcare) for 2 min and then subjected to the imaging system (UVITEC
657 Cambridge) to record signals.

658 Amber codon mutation of selected CouA incorporation sites in
659 pET28A-pBAD-*pmrA*

660 Selective amino acid located in the DNA binding domain of PmrA was subjected to
661 replacement by CouA, each of these CouA incorporation sites were mutated to a TAG
662 amber codon by site-directed mutagenesis PCR. PCR was conducted using a pair of
663 primers for the desired mutagenesis and pET28A-pBAD-*pmrA* plasmid as the template.
664 PCR product was purified using MiniBEST agarose gel DNA extraction kit (TaKaRa).
665 Following DpnI digestion of the template for 16 hrs, the PCR product was transformed into
666 *E. coli* DH5α. Transformants were recovered on LB agar plates supplemented with
667 kanamycin (20 μg/ml) at 37°C overnight. Colonies recovered were verified by DNA
668 sequencing (BGI, Shenzhen).

669 In vivo $PmrA_{CouA}$ - $promoter_{SYTO\ 9}$ binding assay

670 Binding of $PmrA_{CouA}$ and $promoter_{SYTO\ 9}$ was monitored by FRET assay following our
671 previous description with minor modifications[43]. Plasmid pET28a-pBAD-*pmrA*-G137TAG
672 was co-transformed with pEVOL-CouRS into *E. coli* MG1655 *ΔpmrA* strain, resulting in
673 AY7065 constructs. A fresh single colony of AY7065 was inoculated into MOPS medium
674 supplemented with kanamycin (20 μg/ml) and chloramphenicol (25 μg/ml) and grew
675 overnight at 37°C. 75 μl of the overnight culture was inoculated to 7.5 ml fresh medium to

676 subculture the bacteria. Following culturing at 37°C for 4 hrs, CouA incorporation and
677 expression of PmrA-G137CouA was induced mildly by supplementing 0.9% arabinose
678 and 1mM CouA at 37°C for 5 hrs. Approximately 3.5×10^{10} cells were harvested and
679 washed twice with fresh MOPS medium. Cells were resuspended in MOPS medium as
680 control, or MOPS medium supplemented with 0.5 mM $FeSO_4$, or Pi- MOPS medium and
681 shake for 1 hr at 37°C. After centrifugation at 4500 rpm for 15 min at 4°C, cell pellet was
682 resuspended in 600 μl of PBS. 85 μl of the suspension was added in each of 6 wells (3
683 wells for control and 3 wells for experimental group) on a 96-well black plate preloaded
684 with 15 μl of 50 μM SYTO 9 and was incubated for 15 min at room temperature in the dark
685 before being subjected to fluorescence recording (Thermo Scientific Varioskan® Flash
686 spectral scanning multimode reader).

687 Comparative proteomic analysis

688 *E. coli* MG1655 cultured in MOPS medium to OD_{600} of 0.5 was harvested as cells under
689 Pi sufficient condition. The same volume of cells was washed with Pi depletion medium
690 for 3times and resuspended in Pi depletion medium and shake for 3 hrs at 37°C as cells
691 subjected to Pi depletion. Each type of cell pellets with three biological replicates were
692 lysed by resuspending in 20 μl BugBuster reagent (Novagen, USA) (containing 25 mg/ml
693 lysozyme, 1 unit DNase I) at room temperature for 30 mins following centrifugation at
694 13000 rpm at 4°C for 20 min. Supernatant was transferred to a clean microcentrifuge tube
695 and mixed with 4×SDS sample buffer (40% glycerol, 8% SDS, 240 mM Tris/HCl pH 6.8,
696 0.04% bromophenol blue) supplemented with 5% β-mercaptoethanol. Sample were

697 incubated at 55 °C for 25 min. 20 μL of each sample were loaded onto a polyacrylamide
698 gel composed of a 10% resolving (lower) gel and a 6% stacking (upper) gel following
699 staining with Coomassie blue staining and fractionated into eight fractions. Gel slices were
700 cut into 1 mm^3 cubes and destained with 50% acetonitrile (ACN) in 50 mm triethyl
701 ammonium bicarbonate (TEAB) and dehydrated with pure CAN and dried in a vacuum
702 concentrator. Sequencing grade modified trypsin (Promega) diluted by an ice-cold buffer
703 containing 50 mM NH4HCO3 and 10% (v/v) ACN was added to cover the dehydrated gel
704 pieces on ice. After 30 min, more trypsin-containing buffer was added to cover the
705 expanded gel pieces followed by overnight incubation at 37 °C. Finally, the resulting tryptic
706 peptides were extracted from the gel by equilibrating the samples with 50% ACN and 5%
707 formic acid (FA) for 20 min in a 37 °C shaker. The extraction was repeated once, and all
708 fractions were combined and vacuum dried. The protein digest was resuspended in 100
709 μl of 100 mm TEAB, and then 4 μl of 0.6 m sodium cyanoborohydride ($NaBH_3CN$) were
710 added. Peptides from PI+ and Pi- were labeled with 4 μl of 4% formaldehyde (CH_2O) and
711 deuterated formaldehyde (CD_2O), respectively. The reaction mixture was vortexed and
712 incubated at room temperature for 1 h. The reaction was quenched by sequential addition
713 of 16 μl of 1% (v/v) ammonia solution and 8 μl of formic acid. Finally, light- and heavy-
714 labeled peptides were mixed, and vacuum dried immediately before further mass
715 spectrometric analyses. Extracted peptides were analyzed by Nanoflow LC-MS/MS
716 analyses using the EASY-nLC 1000 System (Thermo Scientific, USA) and LTQ Velos
717 (Thermo Scientific, USA).

718 Data processing was performed following a previous description[70]. For protein
719 identification, MS/MS spectra were extracted from RAW files using MaxQuant
720 (http://maxquant.org/, version 1.5.3.30). MASCOT (Matrix Science, version 2.3.02) was
721 used to perform database search against an *E. coli* database (strain MG1655, with
722 sequence files downloaded from UniProt in FASTA format, 4,358 entries. Average mass
723 was selected with precursor mass tolerance of 1.5 Da and fragment mass tolerance of 0.8
724 Da. Methionine oxidation was set as a dynamic modification. The resulting assignments
725 were filtered to achieve a false-discovery rate (FDR) of <1% at both the peptide and
726 protein levels using the target-decoy method. Relative abundances of protein were
727 represented by spectral counts, which are the number of repeated identification of
728 peptides during the entire analysis.

729 To identify proteins that were differentially expressed in the sets of samples, the spectral
730 counts data were subjected to statistic by DESeq package (Anders and Huber 2010) in R
731 (Team 2014). Briefly, to eliminate the variance caused by sample loading and machine
732 reading depth, the total counts data of two biological conditions was normalized to the
733 same size. The following statistics were performed: *foldChange* (fold change from
734 condition A to B), *pval* (p value for the statistical significance of this change), and *padj* (p
735 value adjusted for multiple testing with the Benjamini-Hochberg procedure, which controls
736 false discovery rate). Data set with *padj* <0.05 were considered to be significant (Anders
737 and Huber 2010), and corresponding proteins were listed in S1 Table.

738 **Polymyxin challenging assay**

739 Challenging *E .coli* cells with designated concentration of polymyxin B (Sigma. USA) were
740 performed as described with modifications.[71] *E. coli* cells grown under designated
741 conditions were harvested by centrifugation at 13000 rpm for 1min. Cell pellets were re-
742 suspended in MOPS medium to a final concentration of 10^8 cells/ml. The cell culture was
743 treated with polymyxin B with designated concentration for 1-3 hours at 37 °C without
744 agitation. Cell culture prior to and following polymyxin treatment was plated on LB plate,
745 CFU was counted after 12-16 hours incubation at 37°C. Survival of polymyxin challenging
746 was determined by the survival rate of *E. coli* cells after drug treatment. Results are
747 presented as the mean of three biological replicates.

748 Phylogenetic analysis of EcoPmrB homologs

749 The PmrB sequences from *E. coli* K-12 MG1655 were used as a query against γ-
750 proteobacteria via BLASTP searches in the UniProt database, with an E-threshold of 10
751 and the BLOSUM62 substitution matrix. The top 250 retrieved sequences were aligned
752 using the MUSCLE algorithm implemented in MEGA12 software. A phylogenetic tree of
753 EcoPmrB homologous was constructed using the Maximum Likelihood method, with
754 branch support assessed via adaptive bootstrap analysis using 562 bootstrap replicates
755 in MEGA12. The JTT model was applied as the evolutionary model for tree construction.

756 Statistical analysis

757 Statistical analysis was performed using GraphPad Prism. Group comparisons between
758 two groups were performed using two-tailed Student's *t* test. Group comparisons between

759 multiple groups were performed using one-way ANOVA or two-way ANOVA with post hoc
760 tests.

761 Acknowledgments

762 We thank Ms. Yining Chen in Prof. A. Yan's lab for proofreading the manuscript. We thank
763 Prof. Changhao Bi (Tianjin Institute of Industrial Biotechnology, Chinese Academy of
764 Sciences) for the generous gift of pCAGO plasmid. We thank Prof. Zhaochao Xu and Prof.
765 Lu Miao (CAS Key Laboratory of Separation Science for Analytical Chemistry, Dalian
766 Institute of Chemical Physics, Chinese Academy of Sciences) for the generous gift of OM-
767 sensitive probe PI-BactD. We thank Prof. Patrick C. Y. Woo (Department of Microbiology,
768 University of Hong Kong) for the generous gift of clinical *E. coli* strains.

769 Funding

770 This work was supported by the
771 Research Grants Council of Hong Kong, Theme-based Research Scheme T21-705/20-N
772 (A.Y. and T.Z.)
773 Natural Science Foundation of China 22193062 (T.Z.)
774 Research Grants Council of Hong Kong, Collaborative Research Fund C7033-20G (A.Y.)
775 National Key Research and Development Program of China 2022YFA1304500 (X.L.)
776 Natural Science Foundation of China 22174003 and 21974002 (X.L.)

Author contributions

Conceptualization: Guangming Zhang, Ziqing Deng, Aixin Yan.

Investigation Guangming Zhang, Ziqing Deng, Jiezhang Jiang, Minji Wang, Xiaoyuan Wang, Xiaoyun Liu, Aixin Yan.

Formal Analysis Guangming Zhang, Ziqing Deng, Xiaoyuan Wang, Xiaoyun Liu, Aixin Yan.

Funding Acquisition: Xiaoyun Liu, Aixin Yan.

Resources: Xiaoyuan Wang, Xiaoyun Liu, Aixin Yan.

Supervision: Xiaoyuan Wang, Xiaoyun Liu, Aixin Yan.

Visualization: Guangming Zhang.

Writing – original draft: Guangming Zhang, Aixin Yan.

Writing – review & editing: Guangming Zhang, Xiaoyun Liu, Aixin Yan.

Conflicts of interest

Authors declare that they have no competing interests.

Data and materials availability

All data are available in the main text or the supplementary materials.

References

1. Fang, F.C., Frawley, E.R., Tapscott, T., and Vázquez-Torres, A. (2016). Bacterial stress responses during host infection. Cell host & microbe 20, 133–143.
2. Poole, K. (2012). Bacterial stress responses as determinants of antimicrobial resistance. Journal of Antimicrobial Chemotherapy 67, 2069–2089.
3. Wanner, B.L. (1996). Phosphorus assimilation and control of the phosphate regulon. Escherichia coli and Salmonella: cellular and molecular biology 1, 1357–1381.
4. Fagerbakke, K.M., Heldal, M., and Norland, S. (1996). Content of carbon, nitrogen, oxygen, sulfur and phosphorus in native aquatic and cultured bacteria. Aquatic Microbial Ecology 10, 15–27.
5. Moore, C., Mills, M., Arrigo, K., Berman-Frank, I., Bopp, L., Boyd, P., Galbraith, E., Geider, R., Guieu, C., and Jaccard, S. (2013). Processes and patterns of oceanic nutrient limitation. Nature geoscience 6, 701–710.
6. Van Mooy, B.A., Fredricks, H.F., Pedler, B.E., Dyhrman, S.T., Karl, D.M., Koblížek, M., Lomas, M.W., Mincer, T.J., Moore, L.R., and Moutin, T. (2009). Phytoplankton in the ocean use non-phosphorus lipids in response to phosphorus scarcity. Nature 458, 69–72.
7. Vitousek, P.M., Porder, S., Houlton, B.Z., and Chadwick, O.A. (2010). Terrestrial phosphorus limitation: mechanisms, implications, and nitrogen–phosphorus interactions. Ecological applications 20, 5–15.
8. George, T.S., Hinsinger, P., and Turner, B.L. (2016). Phosphorus in soils and plants – facing phosphorus scarcity. Plant and Soil 401, 1–6. 10.1007/s11104-016-2846-9.
9. Nguyen, T.H., Wang, B.X., Diaz, O.R., Rajendram, M., McKenna, J.A., Butler, D.S.C., Hokamp, K., Hinton, J.C.D., Monack, D.M., and Huang, K.C. (2025). Profiling Salmonella transcriptional dynamics during macrophage infection using a comprehensive reporter library. Nature Microbiology 10, 1006–1023. 10.1038/s41564-025-01953-5.
10. Röder, J., Felgner, P., and Hensel, M. (2021). Single-cell analyses reveal phosphate availability as critical factor for nutrition of Salmonella enterica within mammalian host cells. Cell Microbiol 23, e13374. 10.1111/cmi.13374.
11. Jones, R.A., Shropshire, H., Zhao, C., Murphy, A., Lidbury, I., Wei, T., Scanlan, D.J., and Chen, Y. (2021). Phosphorus stress induces the synthesis of novel glycolipids in *Pseudomonas aeruginosa* that confer protection against a last-resort antibiotic. ISME J 15, 3303–3314. 10.1038/s41396-021-01008-7.
12. Ferreira, R.B.R., Antunes, L.C.M., and Sal-Man, N. (2025). Pathogen-pathogen interactions during co-infections. Isme j 19. 10.1093/ismejo/wraf104.
13. Murdoch, C.C., and Skaar, E.P. (2022). Nutritional immunity: the battle for nutrient metals at the host–pathogen interface. Nature Reviews Microbiology 20, 657–670. 10.1038/s41579-022-00745-6.
14. Rossi, E., Falcone, M., Molin, S., and Johansen, H.K. (2018). High-resolution in situ transcriptomics of Pseudomonas aeruginosa unveils genotype independent

835 patho-phenotypes in cystic fibrosis lungs. Nature Communications 9, 3459.
836 10.1038/s41467-018-05944-5.
837 15. Sun, N., Song, Y., Liu, C., Liu, M., Yu, L., and Wang, F. (2021). Analysis of In Vivo
838 Transcriptome of Intracellular Bacterial Pathogen Salmonella enterica serovar
839 Typhmurium Isolated from Mouse Spleen. Pathogens 10.
840 10.3390/pathogens10070823.
841 16. Makino, K., Shinagawa, H., Amemura, M., Kawamoto, T., Yamada, M., and Nakata,
842 A. (1989). Signal transduction in the phosphate regulon of *Escherichia coli* involves
843 phosphotransfer between PhoR and PhoB proteins. Journal of molecular biology
844 210, 551–559.
845 17. Hsieh, Y.-J., and Wanner, B.L. (2010). Global regulation by the seven-component
846 Pi signaling system. Current opinion in microbiology 13, 198–203.
847 18. Crépin, S., Chekabab, S.-M., Le Bihan, G., Bertrand, N., Dozois, C.M., and Harel,
848 J. (2011). The Pho regulon and the pathogenesis of *Escherichia coli*. Veterinary
849 microbiology 153, 82–88.
850 19. Chekabab, S.M., Harel, J., and Dozois, C.M. (2014). Interplay between genetic
851 regulation of phosphate homeostasis and bacterial virulence. Virulence 5, 786–793.
852 20. Romano, S., Schulz-Vogt, H.N., González, J.M., and Bondarev, V. (2015).
853 Phosphate limitation induces drastic physiological changes, virulence-related gene
854 expression, and secondary metabolite production in *Pseudovibrio* sp. strain FO-
855 BEG1. Applied and environmental microbiology 81, 3518–3528.
856 21. Pratt, J.T., Ismail, A.M., and Camilli, A. (2010). PhoB regulates both environmental
857 and virulence gene expression in *Vibrio cholerae*. Molecular microbiology 77,
858 1595–1605.
859 22. Jensen, V., Löns, D., Zaoui, C., Bredenbruch, F., Meissner, A., Dieterich, G., Münch,
860 R., and Häussler, S. (2006). RhlR expression in *Pseudomonas aeruginosa* is
861 modulated by the *Pseudomonas* quinolone signal via PhoB-dependent and-
862 independent pathways. Journal of bacteriology 188, 8601–8606.
863 23. Ferreira, G.M., and Spira, B. (2008). The pst operon of enteropathogenic
864 *Escherichia coli* enhances bacterial adherence to epithelial cells. Microbiology 154,
865 2025–2036.
866 24. Romanowski, K., Zaborin, A., Fernandez, H., Poroyko, V., Valuckaite, V., Gerdes,
867 S., Liu, D.C., Zaborina, O.Y., and Alverdy, J.C. (2011). Prevention of siderophore-
868 mediated gut-derived sepsis due to *P. aeruginosa* can be achieved without iron
869 provision by maintaining local phosphate abundance: role of pH. BMC microbiology
870 11, 1–14.
871 25. Santos-Beneit, F., and Martin, J.F. (2013). Vancomycin resistance in *Streptomyces*
872 *coelicolor* is phosphate-dependent but is not mediated by the PhoP regulator. J
873 Glob Antimicrob Resist 1, 109–113. 10.1016/j.jgar.2013.03.003.
874 26. Dorrer, E., and Teuber, M. (1977). Induction of polymyxin resistance in
875 *Pseudomonas fluorescens* by phosphate limitation. Archives of Microbiology 114,
876 87–89.
877 27. Olea-Ozuna, R.J., Campbell, M.J., Quintanilla, S.Y., Nandy, S., Brodbelt, J.S., and

Boll, J.M. (2025). Alternative lipid synthesis in response to phosphate limitation promotes antibiotic tolerance in Gram-negative ESKAPE pathogens. PLoS pathogens 21, e1012933.

28. Lewenza, S., Falsafi, R., Bains, M., Rohs, P., Stupak, J., Sprott, G.D., and Hancock, R.E. (2011). The *olsA* gene mediates the synthesis of an ornithine lipid in *Pseudomonas aeruginosa* during growth under phosphate-limiting conditions, but is not involved in antimicrobial peptide susceptibility. FEMS Microbiol Lett 320, 95–102. 10.1111/j.1574-6968.2011.02295.x.
29. Barbosa, L.C., Goulart, C.L., Avellar, M.M., Bisch, P.M., and von Kruger, W.M.A. (2018). Accumulation of ornithine lipids in Vibrio cholerae under phosphate deprivation is dependent on VC0489 (OlsF) and PhoBR system. Microbiology (Reading) 164, 395–399. 10.1099/mic.0.000607.
30. Geiger, O., Röhrs, V., Weissenmayer, B., Finan, T.M., and Thomas-Oates, J.E. (1999). The regulator gene phoB mediates phosphate stress-controlled synthesis of the membrane lipid diacylglyceryl-N,N,N-trimethylhomoserine in Rhizobium (Sinorhizobium) meliloti. Mol Microbiol 32, 63–73. 10.1046/j.1365-2958.1999.01325.x.
31. Lev, S., Rupasinghe, T., Desmarini, D., Kaufman-Francis, K., Sorrell, T.C., Roessner, U., and Djordjevic, J.T. (2019). The PHO signaling pathway directs lipid remodeling in Cryptococcus neoformans via DGTS synthase to recycle phosphate during phosphate deficiency. PLoS One 14, e0212651. 10.1371/journal.pone.0212651.
32. Geske, T., Vom Dorp, K., Dörmann, P., and Hölzl, G. (2013). Accumulation of glycolipids and other non-phosphorous lipids in Agrobacterium tumefaciens grown under phosphate deprivation. Glycobiology 23, 69–80. 10.1093/glycob/cws124.
33. Gray, R.M., Hunt, D.M., Silva dos Santos, M., Liu, J., Agapova, A., Rodgers, A., Fearns, A., Canseco, J.O., Garza-Garcia, A., MacRae, J.I., et al. (2025). Mycobacterium tuberculosis overcomes phosphate starvation by extensively remodelling its lipidome with phosphorus-free lipids. Nature Communications 16, 11317. 10.1038/s41467-025-66437-w.
34. Vences-Guzman, M.A., Geiger, O., and Sohlenkamp, C. (2012). Ornithine lipids and their structural modifications: from A to E and beyond. FEMS microbiology letters 335, 1–10.
35. Sohlenkamp, C., and Geiger, O. (2016). Bacterial membrane lipids: diversity in structures and pathways. FEMS microbiology reviews 40, 133–159.
36. Kiriukhin, M.Y., Debabov, D.V., Shinabarger, D.L., and Neuhaus, F.C. (2001). Biosynthesis of the glycolipid anchor in lipoteichoic acid of *Staphylococcus aureus* RN4220: role of YpfP, the diglucosyldiacylglycerol synthase. Journal of bacteriology 183, 3506–3514.
37. Groat, R.G., Schultz, J., Zychlinsky, E., Bockman, A., and Matin, A. (1986). Starvation proteins in Escherichia coli: kinetics of synthesis and role in starvation survival. Journal of Bacteriology 168, 486–493.
38. Raetz, C.R., Reynolds, C.M., Trent, M.S., and Bishop, R.E. (2007). Lipid A

921 modification systems in gram-negative bacteria. Annu. Rev. Biochem. 76, 295–329.
922 39. Ogasawara, H., Shinohara, S., Yamamoto, K., and Ishihama, A. (2012). Novel
923 regulation targets of the metal-response BasS-BasR two-component system of
924 *Escherichia coli*. Microbiology (Reading) 158, 1482–1492. 10.1099/mic.0.057745-
925 0.
926 40. Fernandez-Ciruelos, B., Potmis, T., Solomin, V., and Wells, J.M. (2023). Cross-talk
927 between QseBC and PmrAB two-component systems is crucial for regulation of
928 motility and colistin resistance in Enteropathogenic Escherichia coli. PLoS Pathog
929 19, e1011345. 10.1371/journal.ppat.1011345.
930 41. Winfield, M.D., and Groisman, E.A. (2004). Phenotypic differences between
931 Salmonella and Escherichia coli resulting from the disparate regulation of
932 homologous genes. Proceedings of the National Academy of Sciences 101,
933 17162–17167.
934 42. Wösten, M.M., Kox, L.F., Chamnongpol, S., Soncini, F.C., and Groisman, E.A.
935 (2000). A signal transduction system that responds to extracellular iron. Cell 103,
936 113–125.
937 43. Wang, P., Zhang, G., Xu, Z., Chen, Z., Liu, X., Wang, C., Zheng, C., Wang, J.,
938 Zhang, H., and Yan, A. (2022). Whole-cell FRET monitoring of transcription factor
939 activities enables functional annotation of signal transduction systems in living
940 bacteria. J Biol Chem, 102258. 10.1016/j.jbc.2022.102258.
941 44. Wang, J., Xie, J., and Schultz, P.G. (2006). A genetically encoded fluorescent
942 amino acid. Journal of the American Chemical Society 128, 8738–8739.
943 45. Chen, H.D., and Groisman, E.A. (2013). The biology of the PmrA/PmrB two-
944 component system: the major regulator of lipopolysaccharide modifications. Annual
945 review of microbiology 67, 83–112.
946 46. Lee, L.J., Barrett, J.A., and Poole, R.K. (2005). Genome-wide transcriptional
947 response of chemostat-cultured Escherichia coli to zinc. Journal of bacteriology
948 187, 1124–1134.
949 47. Alves, E., Moreirinha, C., Faustino, M.A., Cunha, A., Delgadillo, I., Neves, M.G.,
950 and Almeida, A. (2016). Overall biochemical changes in bacteria photosensitized
951 with cationic porphyrins monitored by infrared spectroscopy. Future Medicinal
952 Chemistry 8, 613–628.
953 48. Breuer, W., Epsztejn, S., and Cabantchik, Z.I. (1995). Iron Acquired from
954 Transferrin by K562 Cells Is Delivered into a Cytoplasmic Pool of Chelatable Iron
955 (II)(∗). Journal of Biological Chemistry 270, 24209–24215.
956 49. Long, S., Miao, L., Li, R., Deng, F., Qiao, Q., Liu, X., Yan, A., and Xu, Z. (2019).
957 Rapid Identification of Bacteria by Membrane-Responsive Aggregation of a Pyrene
958 Derivative. ACS Sens 4, 281–285. 10.1021/acssensors.8b01466.
959 50. Huang, J., Li, C., Song, J., Velkov, T., Wang, L., Zhu, Y., and Li, J. (2020).
960 Regulating polymyxin resistance in Gram-negative bacteria: roles of two-
961 component systems PhoPQ and PmrAB. Future microbiology 15, 445–459.
962 51. Hofstaedter, C.E., Chandler, C.E., Met, C.M., Gillespie, J.J., Harro, J.M., Goodlett,
963 D.R., Rasko, D.A., and Ernst, R.K. (2024). Divergent Pseudomonas aeruginosa

964 LpxO enzymes perform site-specific lipid A 2-hydroxylation. Mbio 15, e02823–
965 02823.
966 52. Pontes, M.H., Sevostyanova, A., and Groisman, E.A. (2015). When too much ATP
967 is bad for protein synthesis. Journal of molecular biology 427, 2586–2594.
968 53. Bruna, R.E., Kendra, C.G., Groisman, E.A., and Pontes, M.H. (2021). Limitation of
969 phosphate assimilation maintains cytoplasmic magnesium homeostasis. Proc Natl
970 Acad Sci U S A 118. 10.1073/pnas.2021370118.
971 54. Klein, D.J., Moore, P.B., and Steitz, T.A. (2004). The contribution of metal ions to
972 the structural stability of the large ribosomal subunit. Rna 10, 1366–1379.
973 55. Pontes, M.H., and Groisman, E.A. (2018). Protein synthesis controls phosphate
974 homeostasis. Genes & development 32, 79–92.
975 56. Perez, J.C., Shin, D., Zwir, I., Latifi, T., Hadley, T.J., and Groisman, E.A. (2009).
976 Evolution of a bacterial regulon controlling virulence and Mg^{2+} homeostasis. PLoS
977 genetics 5, e1000428.
978 57. Véscovi, E.G., Soncini, F.C., and Groisman, E.A. (1996). Mg^{2+} as an extracellular
979 signal: environmental regulation of Salmonella virulence. Cell 84, 165–174.
980 58. Breazeale, S.D., Ribeiro, A.A., and Raetz, C.R. (2002). Oxidative decarboxylation
981 of UDP-glucuronic acid in extracts of polymyxin-resistant Escherichia coli: Origin of
982 lipid a species modified with 4-amino-4-deoxy-l-arabinose. Journal of Biological
983 Chemistry 277, 2886–2896.
984 59. Breazeale, S.D., Ribeiro, A.A., and Raetz, C.R. (2003). Origin of Lipid A Species
985 Modified with 4-Amino-4-deoxy-l-arabinose in Polymyxin-resistant Mutants of
986 Escherichia coli: an aminotransferase (ArnB) that generates UDP-4-amino-4-
987 deoxy-l-arabinose. Journal of Biological Chemistry 278, 24731–24739.
988 60. Yan, A., Guan, Z., and Raetz, C.R. (2007). An undecaprenyl phosphate-
989 aminoarabinose flippase required for polymyxin resistance in *Escherichia coli*. J
990 Biol Chem 282, 36077–36089. 10.1074/jbc.M706172200.
991 61. Breazeale, S.D., Ribeiro, A.A., McClerren, A.L., and Raetz, C.R. (2005). A
992 formyltransferase required for polymyxin resistance in Escherichia coli and the
993 modification of lipid A with 4-amino-4-deoxy-l-arabinose: identification and function
994 of UDP-4-deoxy-4-formamido-l-arabinose. Journal of Biological Chemistry 280,
995 14154–14167.
996 62. Gunn, J.S., Lim, K.B., Krueger, J., Kim, K., Guo, L., Hackett, M., and Miller, S.I.
997 (1998). PmrA–PmrB-regulated genes necessary for 4-aminoarabinose lipid A
998 modification and polymyxin resistance. Molecular microbiology 27, 1171–1182.
999 63. Stevenson, G., Andrianopoulos, K., Hobbs, M., and Reeves, P.R. (1996).
1000 Organization of the *Escherichia coli* K-12 gene cluster responsible for production
1001 of the extracellular polysaccharide colanic acid. Journal of bacteriology 178, 4885–
1002 4893.
1003 64. Baijal, K., Abramchuk, I., Herrera, C.M., Mah, T.-F., Trent, M.S., Lavallée-Adam, M.,
1004 and Downey, M. (2024). Polyphosphate kinase regulates LPS structure and
1005 polymyxin resistance during starvation in E. coli. Plos Biology 22, e3002558.
1006 65. Dahal, P. (2022). Enterobacteriaceae-definition, characteristics, identification.

1007 Microbe Notes.
1008 66. Bligh, E.G., and Dyer, W.J. (1959). A rapid method of total lipid extraction and
1009 purification. Canadian journal of biochemistry and physiology 37, 911–917.
1010 67. Sahonero-Canavesi, D.X., López-Lara, I.M., and Geiger, O. (2019). Membrane lipid
1011 degradation and lipid cycles in microbes. Aerobic Utilization of Hydrocarbons, Oils,
1012 and Lipids 10, 978–973.
1013 68. Xu, Z., Wang, P., Wang, H., Yu, Z.H., Au-Yeung, H.Y., Hirayama, T., Sun, H., and
1014 Yan, A. (2019). Zinc excess increases cellular demand for iron and decreases
1015 tolerance to copper in *Escherichia coli*. J Biol Chem 294, 16978–16991.
1016 10.1074/jbc.RA119.010023.
1017 69. Zhao, D., Feng, X., Zhu, X., Wu, T., Zhang, X., and Bi, C. (2017). CRISPR/Cas9-
1018 assisted gRNA-free one-step genome editing with no sequence limitations and
1019 improved targeting efficiency. Sci Rep 7, 16624. 10.1038/s41598-017-16998-8.
1020 70. Liu, Y., Zhang, Q., Hu, M., Yu, K., Fu, J., Zhou, F., and Liu, X. (2015). Proteomic
1021 analyses of intracellular *Salmonella enterica* serovar Typhimurium reveal extensive
1022 bacterial adaptations to infected host epithelial cells. Infection and immunity 83,
1023 2897–2906.
1024 71. Groisman, E.A., Kayser, J., and Soncini, F.C. (1997). Regulation of polymyxin
1025 resistance and adaptation to low-Mg^{2+} environments. Journal of bacteriology 179,
1026 7040–7045.

1027

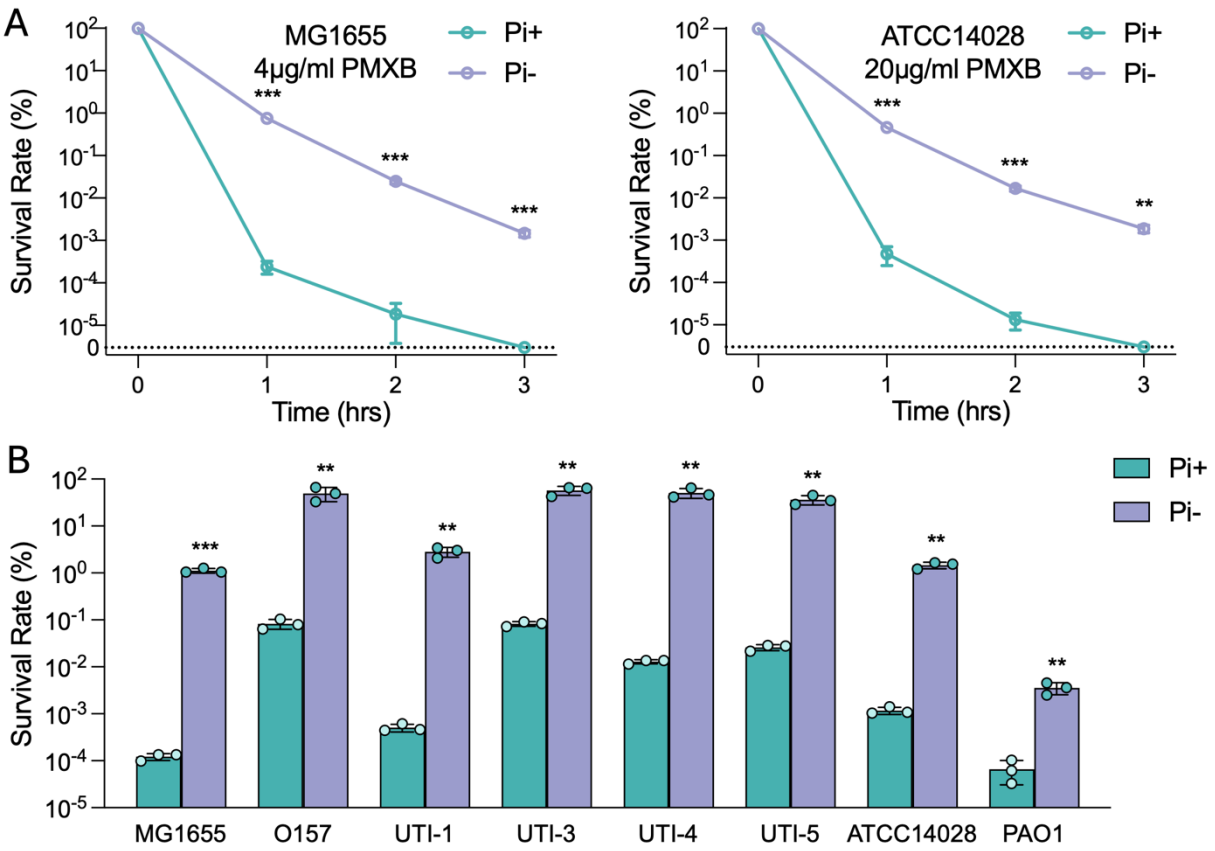

Figure 1. Pi depletion induces polymyxin resistance in diverse bacterial species.

(**A**) Time-kill curves of *Escherichia coli* MG1655 (left panel) and *Salmonella*. Typhimurium ATCC14028 (right panel) exposed to polymyxin B (PMXB) (4 μg/ml for *E. coli* strains, 20 μg/ml for *S.* Typhimurium) following acute Pi-starvation treatment (Pi-, 0 mM Pi) compared to the group without treatment (Pi+, 1.32 mM Pi).

(**B**) Survival rates for various *Enterobacteriaceae* strains (*E. coli* MG1655, O157, UTI-1, UTI-3, UTI-4, UTI-5, *S.* Typhimurium ATCC14028) and *Pseudomonas aeruginosa* PAO1 exposed 1-hour to polymyxin B (4 μg/ml for *E. coli* strains, 20 μg/ml for *S.* Typhimurium and 8 μg/ml for *P. aeruginosa*). For all tested strains, phosphate depletion (Pi-, purple bars) significantly increases polymyxin B resistance compared to phosphate-replete (Pi+, teal bars) conditions.

Error bars represent the standard deviation of at least three independent experiments. Statistical

1040 significance was determined using unpaired two-tailed Student's t-test. Significance levels are

1041 indicated as follows: *$p < 0.05$; **$p < 0.01$; ***$p < 0.001$.

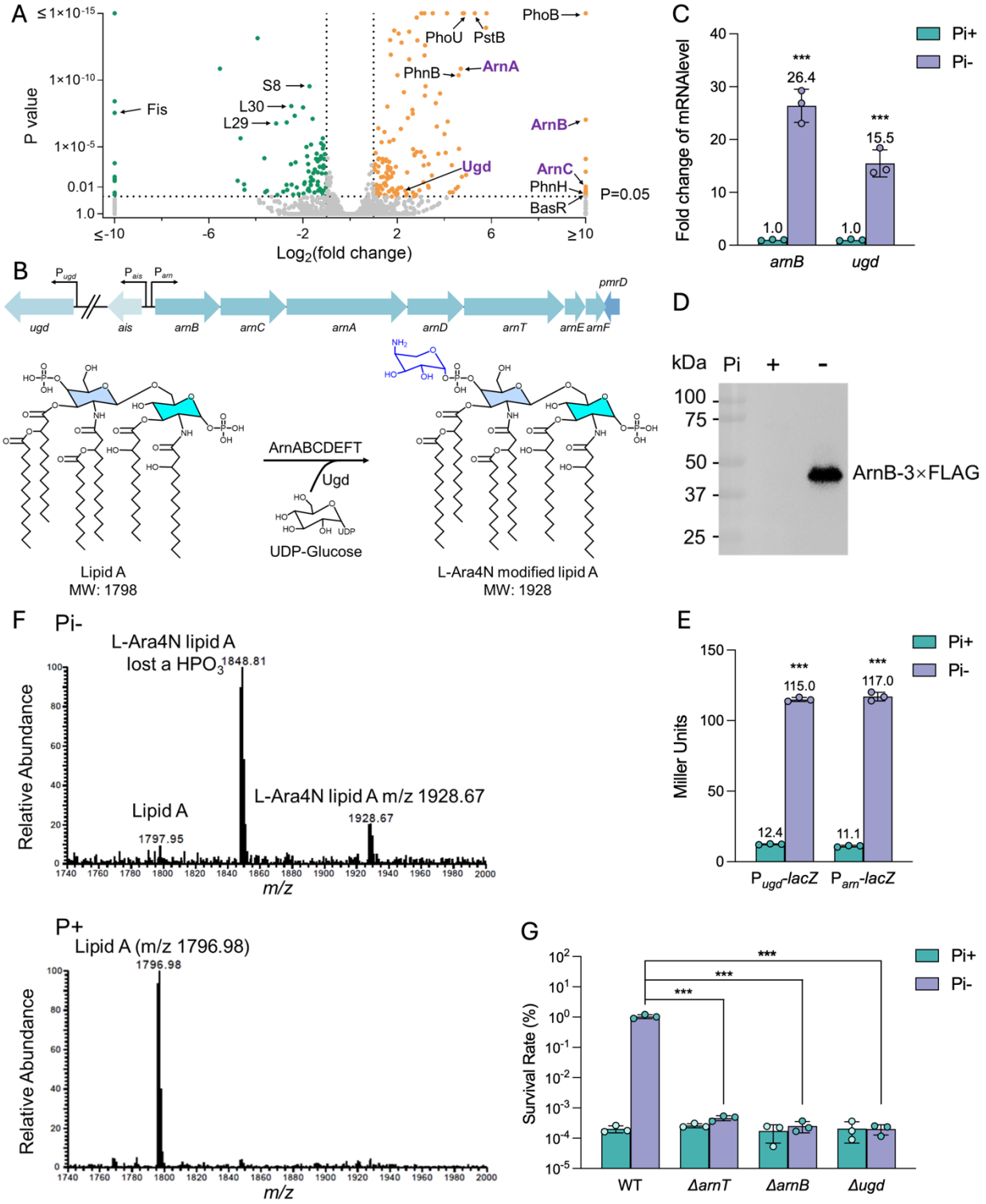

Figure 2. Pi depletion induces the expression of *ugd-arn* system to modify lipid A with L-Ara-4N, conferring stress-induced polymyxin resistance.

1045 (**A**) Volcano plot depicting differentially expressed proteins in cells following acute Pi-starvation
1046 treatment (Pi-, 0 mM) compared to the group without treatment (Pi+, 1.32 mM). Red (right) and
1047 blue (left) dots represent significantly up-regulated and down-regulated proteins, respectively. The
1048 horizontal dashed line depicts a p-value cutoff (0.05), and vertical dashed lines depict 1/2 and 2-
1049 fold ratio cutoffs. Selected proteins are labeled.
1050 (**B**) Genetic organization of the *arn* operon and *ugd* gene in MG1655. Ugd and ArnABCDEFT
1051 catalyze the biosynthesis of 4-amino-4-deoxy-L-arabinose (L-Ara4N) and its modification of lipid
1052 A.
1053 (**C**) mRNA levels of *arnB* and *ugd* in cells following acute Pi-starvation treatment (Pi-, 0 mM)
1054 compared to the group without treatment (Pi+, 1.32 mM).
1055 (**D**) Production of ArnB-3×FLAG in cells following acute Pi-starvation treatment (Pi-, 0 mM)
1056 compared to the group without treatment (Pi+, 1.32 mM). The protein band corresponding to ArnB-
1057 3×FLAG is marked.
1058 (**E**) β-galactosidase activities of P_{arn}-*lacZ* and P_{ugd}-*lacZ* in MG1655 Δ*lacZ* cells following acute Pi-
1059 starvation treatment (Pi-, 0 mM) compared to the group without treatment (Pi+, 1.32 mM).
1060 (**F**) ESI-MS spectra of lipid A molecules extracted from *E. coli* MG1655 cells following acute Pi-
1061 starvation treatment (Pi-, 0 mM) compared to the group without treatment (Pi+, 1.32 mM). Peaks
1062 corresponding to native lipid A and L-Ara-4N modified lipid A were shown.
1063 (**G**) Survival rates for *E. coli* MG1655 parent and isogenic Δ*arnT*, Δ*arnB* and Δ*ugd* mutants
1064 exposed 1-hour to polymyxin B (4 μg/ml) following acute Pi-starvation treatment (Pi-, 0 mM)
1065 compared to the group without treatment (Pi+, 1.32 mM).
1066 Error bars represent the standard deviation of at least three independent experiments. Statistical

1067 significance was determined using two-tailed Student's t-test for **C** and **E**, and one-way ANOVA

1068 followed by Dunnett's multiple comparisons test for **G**. Significance levels are indicated as follows:

1069 *$p < 0.05$; **$p < 0.01$; ***$p < 0.001$.

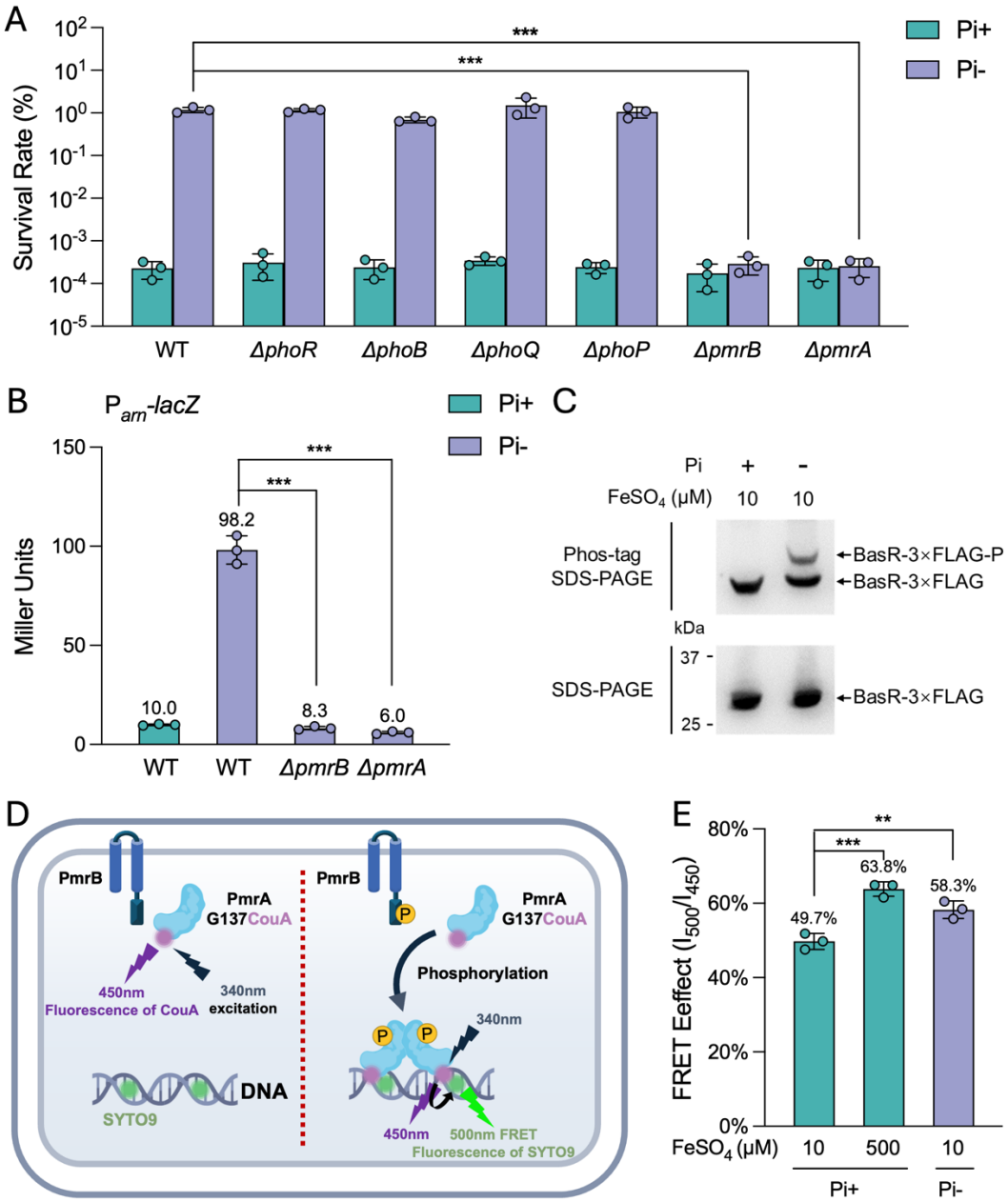

1070

1071 **Figure 3. The PmrAB two-component system is activated during Pi depletion and is**

1072 **responsible for the up-regulation of *arn* genes under this condition.**

1073 (**A**) Survival rates for *E. coli* MG1655 parent and isogenic Δ*pmrB*, Δ*pmrA,* Δ*phoB,* and Δ*phoR*

1074 mutants exposed 1-hour to polymyxin B (4 μg/ml) following acute Pi-starvation treatment (Pi-, 0

1075 mM) compared to the group without treatment (Pi+, 1.32 mM).

1076 (**B**) β-galactosidase activities of P_{arn}-*lacZ* in MG1655 Δ*lacZ* parent and isogenic Δ*pmrB*, Δ*pmrA,*

1077 Δ*phoB,* and Δ*phoR* mutants following acute Pi-starvation treatment (Pi-, 0 mM) compared to the

1078 group without treatment (Pi+, 1.32 mM).

1079 (**C**) Phosphorylation of PmrA-3×FLAG detected by Phos-Tag SDS–PAGE following

1080 immunoblotting with anti-FLAG antibody in cells following acute Pi-starvation treatment (Pi-, 0 mM)

1081 compared to the group without treatment (Pi+, 1.32 mM). Protein bands representing PmrA-

1082 3×FLAG and PmrA-3×FLAG-P are indicated.

1083 (**D**) Schematic diagram of the whole-cell FRET measurement of PmrA-promoter binding assay. A

1084 bright fluorescent unnatural amino acid donor CouA (red spheres) is incorporated into G137 of

1085 PmrA in DNA-binding domain. SYTO9 (green spheres) is employed to stain chromosome DNA in

1086 living *E. coli* MG1655.

1087 (**E**) Quantification of the FRET effect between the CouA-SYTO9 pair in *E. coli* cells following acute

1088 Pi-starvation treatment (Pi-, 0 mM Pi, 10 μM Fe) or iron excess treatment (Pi+, 1.32 mM Pi, 500

1089 μM $FeSO_4$) compared to the group without treatment (Pi+, 1.32 mM Pi, 10 μM $FeSO_4$).

1090 Error bars represent the standard deviation of at least three independent experiments. Statistical

1091 significance was determined using one-way ANOVA followed by Dunnett's multiple comparisons

1092 test for **A**, **B**, and **E**. Significance levels are indicated as follows: *$p < 0.05$; **$p < 0.01$; ***$p < 0.001$.

1093

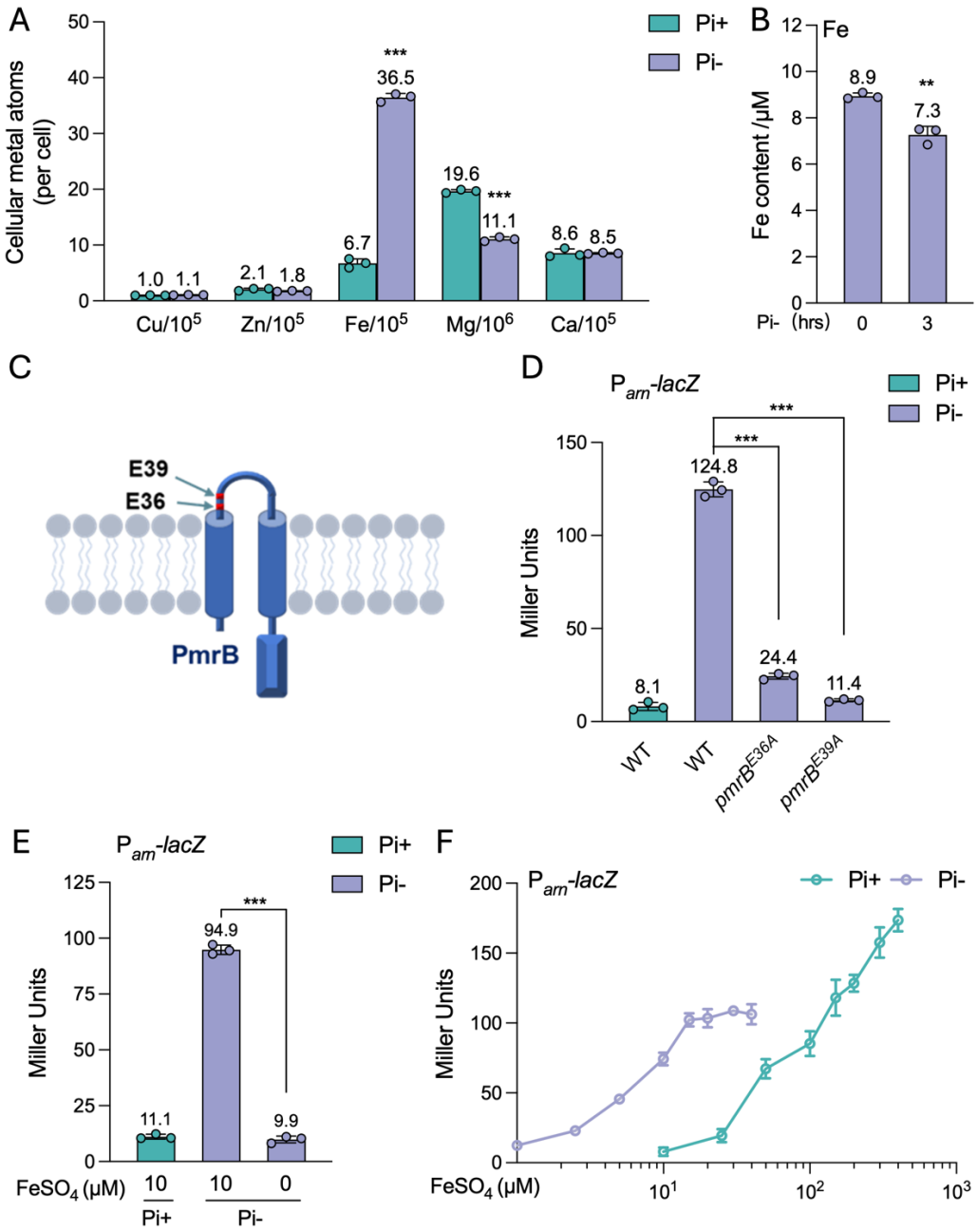

Figure 4. Activation of PmrAB during Pi depletion is mediated by the secondary stress signal iron (Fe^{3+}) induced under this condition

(**A**) Cellular metal contents determined by ICP-MS in *E. coli* MG1655 cells following acute Pi-starvation treatment (Pi-, 0 mM) compared to the group without treatment (Pi+, 1.32 mM).

(**B**) Iron contents in the spent medium of *E. coli* MG1655 at the indicated time points during Pi depletion treatment (Pi-, 0 mM).

1101 (**C**) Schematic diagram of the sensor kinase PmrB. Two important residues for sensing Fe^{3+}, E36A

1102 and E39A, are shown.

1103 (**D**) β-galactosidase activities of P_{arn}-*lacZ* in MG1655 Δ*lacZ* parent and isogenic *pmrB*^{E36A} and

1104 *pmrB*^{E36A} mutants following acute Pi-starvation treatment (Pi-, 0 mM) compared to the group

1105 without treatment (Pi+, 1.32 mM).

1106 (**E**) β-galactosidase activities of P_{arn}-*lacZ* in MG1655 Δ*lacZ* cells following Pi depletion treatment

1107 (Pi-, 0 mM Pi, 10 μM Fe) or Fe, Pi depletion treatment (Pi- Fe-, 0 mM Pi, 0 μM Fe) compared to

1108 the group without treatment (Pi+, 1.32 mM Pi, 10 μM $FeSO_4$).

1109 (**F**) β-galactosidase activities of P_{arn}-*lacZ* in MG1655 Δ*lacZ* grown under Pi sufficient MOPS

1110 medium in the presence of different concentrations of $FeSO_4$ and that subjected to Pi depletion

1111 conditions in the presence of different concentrations of $FeSO_4$.

1112 Error bars represent the standard deviation of at least three independent experiments. Statistical

1113 significance was determined using one-way ANOVA followed by Dunnett's multiple comparisons

1114 test for **B**, and two-tailed Student's t-test for **C**, **D**, and **E**. Significance levels are indicated as

1115 follows: *$p < 0.05$; **$p < 0.01$; ***$p < 0.001$.

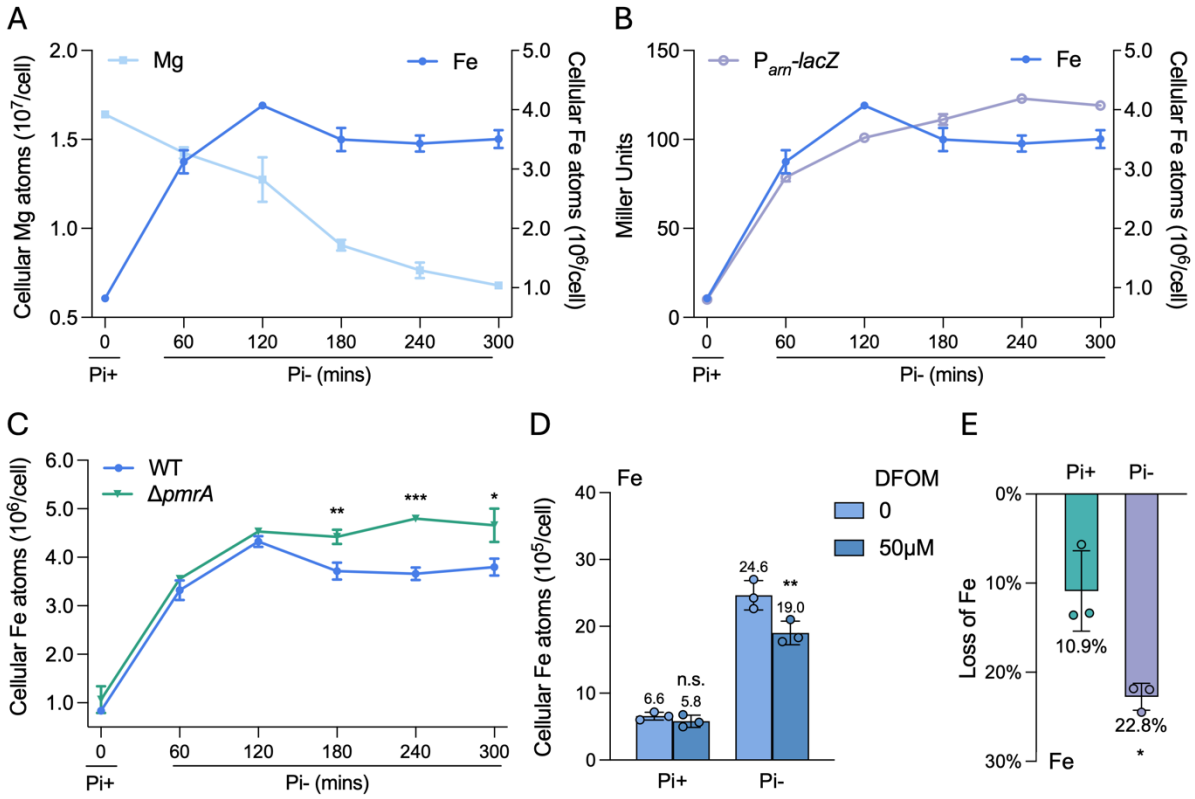

Figure 5. Response to Pi depletion induced iron mobilization to cell surfaces

(**A**) Iron (Fe) and magnesium (Mg) contents in *E. coli* MG1655 cells following Pi depletion treatment (Pi-, 0 mM Pi) at the indicated time points.

(**B**) β-galactosidase activities of P_{arn}-*lacZ* in MG1655 Δ*lacZ* cells and Fe contents in *E. coli* MG1655 cells following Pi depletion treatment at the indicated time points.

(**C**) Fe contents in *E. coli* MG1655 parent and isogenic Δ*pmrA* mutant cells following Pi depletion treatment (Pi-, 0 mM Pi) at the indicated time points.

(**D**) Fe contents in *E. coli* MG1655 cells with Pi depletion treatment (Pi-, 0 mM) and without Pi depletion treatment (Pi+, 1.32 mM) following washing by HEPES or DFOM-supplemented (50μM) HEPES buffer.

(**E**) Reduction of cellular Fe content following washing with DFOM-supplemented (50μM) HEPES

1128 buffer.

1129 Error bars represent the standard deviation of at least three independent experiments. Statistical

1130 significance was determined using two-tailed Student's t-test for **C** and **E**, and two-way ANOVA

1131 followed by Sidak's multiple comparisons test for **D**. Significance levels are indicated as follows:

1132 *$p < 0.05$; **$p < 0.01$; ***$p < 0.001$.

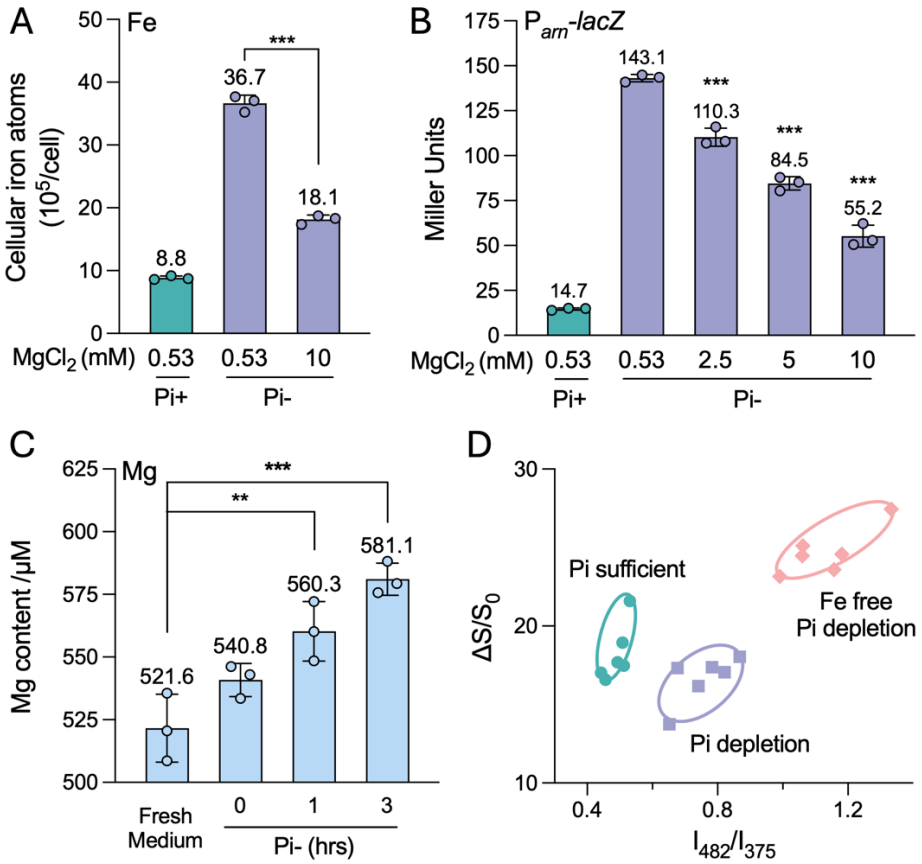

Figure 6. Iron mobilization is driven by Mg^{2+} dissociation during Pi depletion

(**A**) Fe contents in *E. coli* MG1655 cells following acute Pi-starvation treatment (Pi-, 0 mM Pi, 0.53 mM Mg) or Mg excess Pi depletion treatment (Pi-, 0 mM Pi, 10 mM Mg) compared to the group without treatment (Pi+, 1.32 mM, 0.53 mM Mg).

(**B**) β-galactosidase activities of P_{arn}-*lacZ* in MG1655 Δ*lacZ* cells following acute Pi-starvation treatment (Pi-, 0 mM Pi, 0.53 mM Mg) or Mg excess Pi depletion treatment (Pi-, 0 mM Pi, 10 mM Mg) compared to the group without treatment (Pi+, 1.32 mM, 0.53-10 mM Mg).

(**C**) Mg content in the spent medium during Pi depletion treatment at the indicated time points.

(**D**) 2D graph plotted from output signals of two channels of the PI-BactD sensor: fluorescence increase (ΔS/S0) and fluorescence radiometric changes (I482/I375) in each of the treatments

1144 indicated. Data are presented as mean ± s.d. of three biological replicates for **A**, **B**, and **C**, and

1145 six biological replicates for **D**.

1146 Error bars represent the standard deviation of at least three independent experiments. Statistical

1147 significance was determined using two-tailed Student's t-test for **a**, and one-way ANOVA followed

1148 by Dunnett's multiple comparisons test for **B** and **C**. Significance levels are indicated as follows:

1149 *$p < 0.05$; **$p < 0.01$; ***$p < 0.001$.

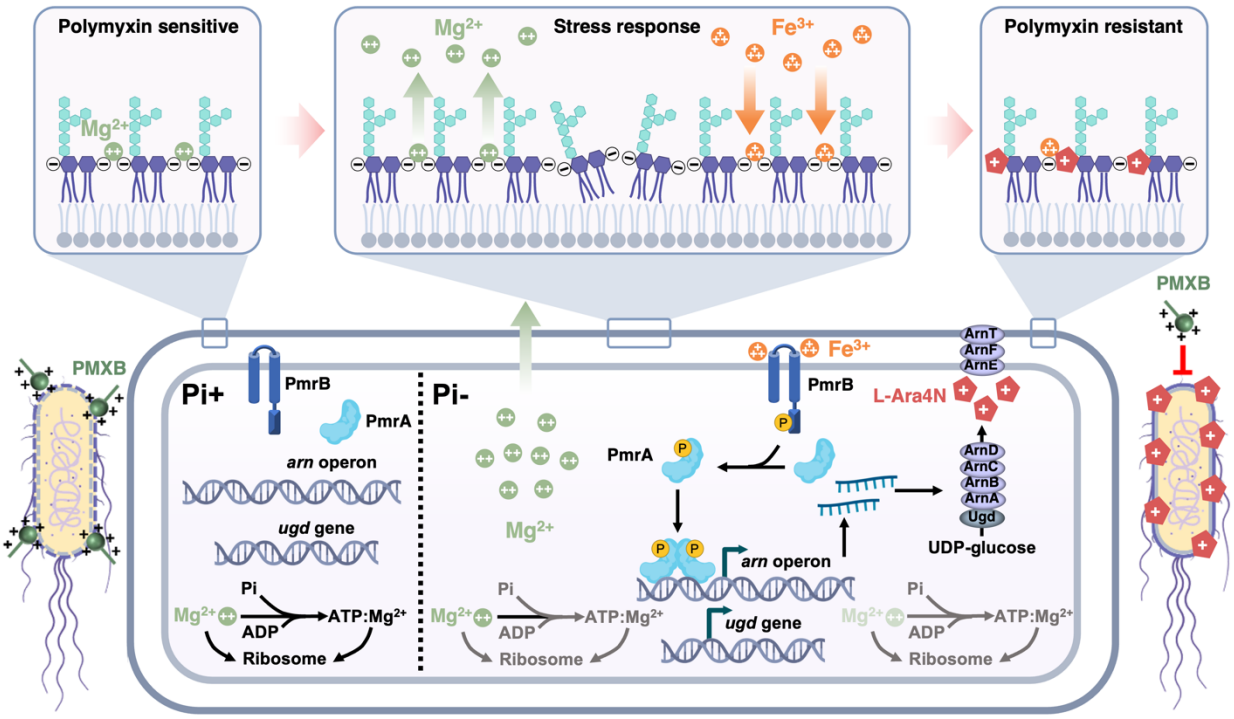

Figure 7. A Mg-Fe-PmrAB regulatory circuit underpins the Pi-depletion induced polymyxin resistance through activating the lipid A L-Ara4N modification system

In cell grown under Pi sufficient condition, ribosome and ATP serve as the major intracellular Mg^{2+} and Pi reservoir. Mg^{2+} neutralizes negative charge of lipid A and stabilizes outer membrane (OM). The PmrAB two-component system (TCS) is inactive, and the cell is sensitive to polymyxin. During Pi stress, ATP biosynthesis and ribosome biogenesis are halted due to Pi depletion, disrupting the balance between Pi and Mg^{2+}. Mg^{2+} disassociates from the cell which destabilizes the OM and derives compensatory Fe^{3+} mobilization to cell surface. Mobilized Fe^{3+} activates the PmrAB TCS which in turn upregulates the *arn* operon. Arn and Ugd proteins catalyze the biosynthesis of L-Arn4N and modify lipid A with L-Arn4N to stabilize OM under stressed condition and prevent further Fe mobilization. *E. coli* cells with L-Arn4N modified lipid A become resistant to polymyxin.

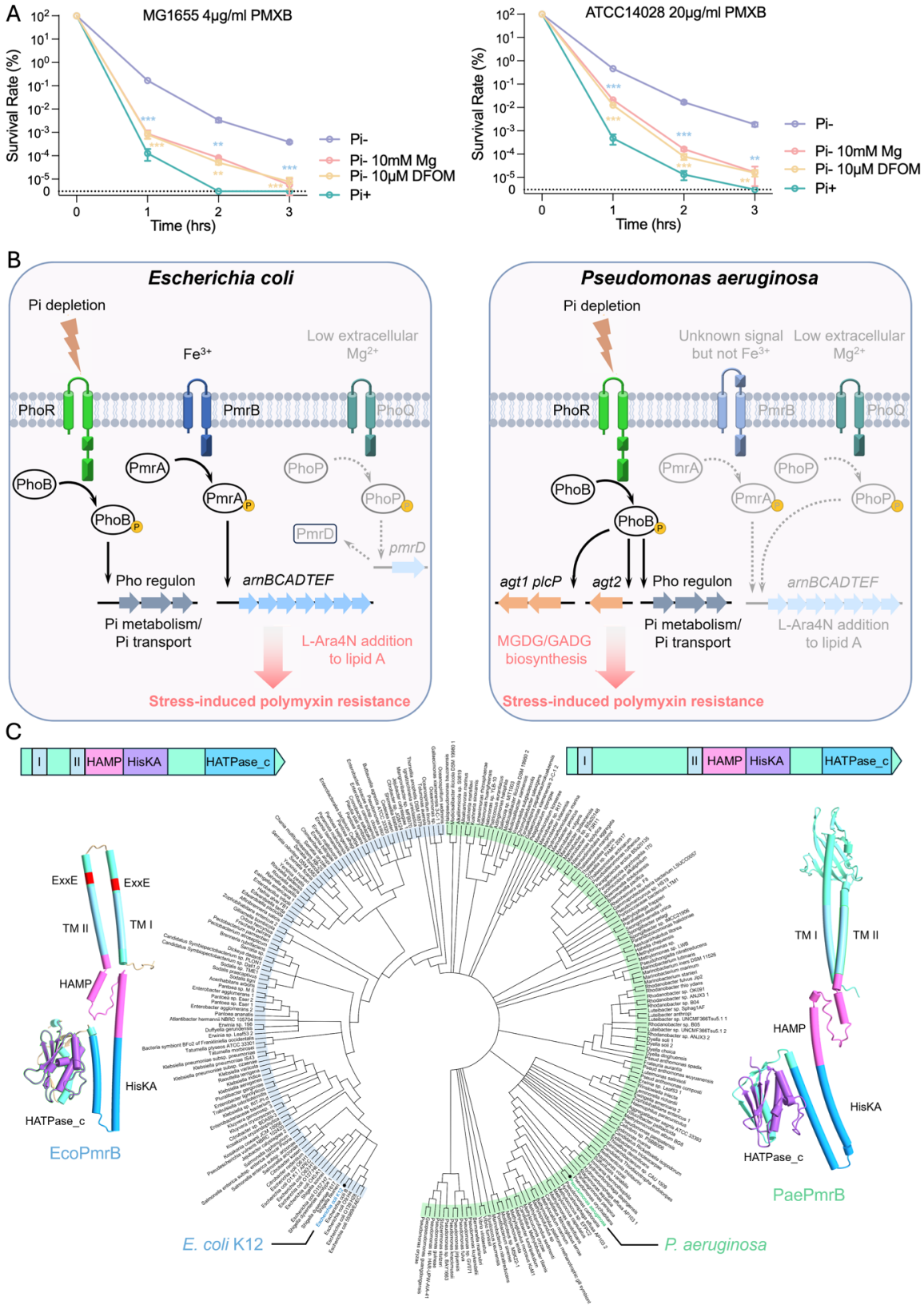

Figure 8. Disrupting the Mg-Fe-PmrAB signaling circuit abolished Pi-depletion induced polymyxin resistance in *Enterobacteriaceae*

1166 (**A**) Time-kill curves of *Escherichia coli* MG1655 (left panel) and *Salmonella*. Typhimurium
1167 ATCC14028 (right panel) exposed to polymyxin B (PMXB) (4 μg/ml for *E. coli* strains, 20 μg/ml for
1168 *S.* Typhimurium) following acute Pi-starvation treatment (Pi-, 0 mM Pi), Pi depletion treatment with
1169 excess Mg (Pi-, 0 mM Pi, 10mM $MgCl_2$) or Pi depletion treatment with iron chelator (Pi-, 0 mM Pi,
1170 10 μM DFOM) compared to the group without treatment (Pi+, 1.32 mM Pi).
1171 (**B**) Distinct stress adaptation strategies in *E. coli* and *P. aeruginosa* under Pi depletion conditions.
1172 Genes and regulatory systems activated in the two species are illustrated. Inactive regulatory
1173 systems are depicted in faded effects. The regulatory mechanisms for *P. aeruginosa* are based
1174 on findings from Jones et. al.[11]
1175 (**C**) A phylogenetic tree of 250 PmrB homologous. A predominant clade is indicated by a blue circle,
1176 comprising sequences from bacteria such as *Escherichia, Shigella, Citrobacter, Salmonella,*
1177 *Klebsiella, Yersinia*, and *Enterobacter* species. A green circle marks several clades distinct from
1178 the predominant one. The domain architecture and AlphaFold3-predicted structure of EcoPmrB
1179 and PaePmrB are shown.

1180 Error bars represent the standard deviation of at least three independent experiments. Statistical
1181 significance was determined using one-way ANOVA followed by Dunnett's multiple comparisons
1182 test. Significance levels are indicated as follows: $*p < 0.05$; $**p < 0.01$; $***p < 0.001$.

Supporting information

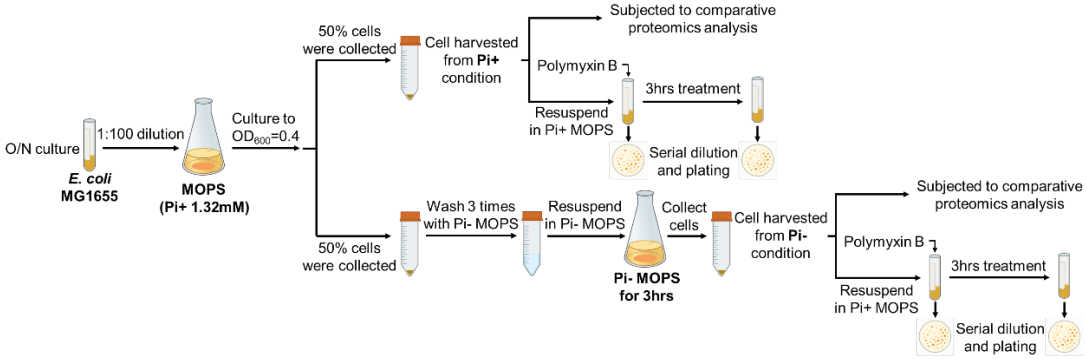

Figure S1. Workflow of acute Pi depletion treatment and following proteomic sample preparation and polymyxin B challenging assay.

Bacteria were cultured to an OD_{600} of 0.4 in standard MOPS synthetic medium containing 1.32 mM inorganic phosphate (Pi), representing Pi-sufficient conditions. For Pi-depletion conditions, bacteria were first grown to OD_{600} = 0.4 in the same medium, then transferred to Pi-depleted MOPS medium (0 mM Pi). For comparative proteomic analysis, the collected bacterial cells were subjected to sample preparation and proteomic analysis. For the polymyxin challenging assay, the collected bacterial cells were resuspended in standard MOPS medium and treated with the designated concentration of polymyxin B. Cell viability was assessed at the beginning and end of treatment by serial dilution and plating.

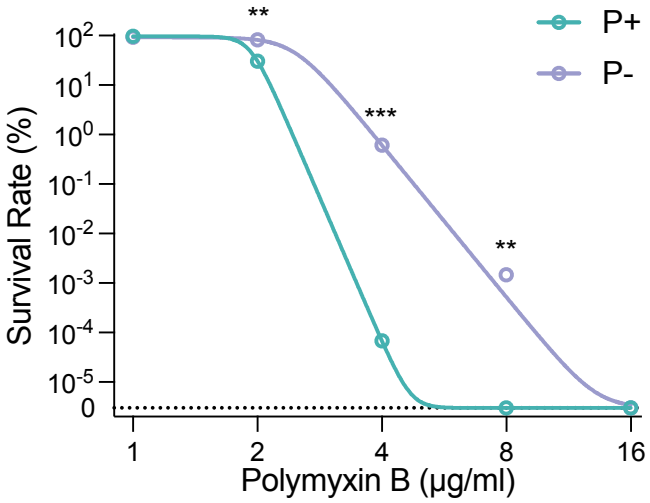

Figure S2. Killing of *E. coli* MG1655 with different concentration of polymyxin B.

Survival rates for *E. coli* MG1655 cells exposed 1-hour to polymyxin B (1-16 μg/ml) following acute Pi-starvation treatment (Pi-, 0 mM) compared to the group without treatment (Pi+, 1.32 mM). Error bars represent the standard deviation of at least three independent experiments. Statistical significance was determined using unpaired two-tailed Student's t-test. Significance levels are indicated as follows: *$p < 0.05$; **$p < 0.01$; ***$p < 0.001$.

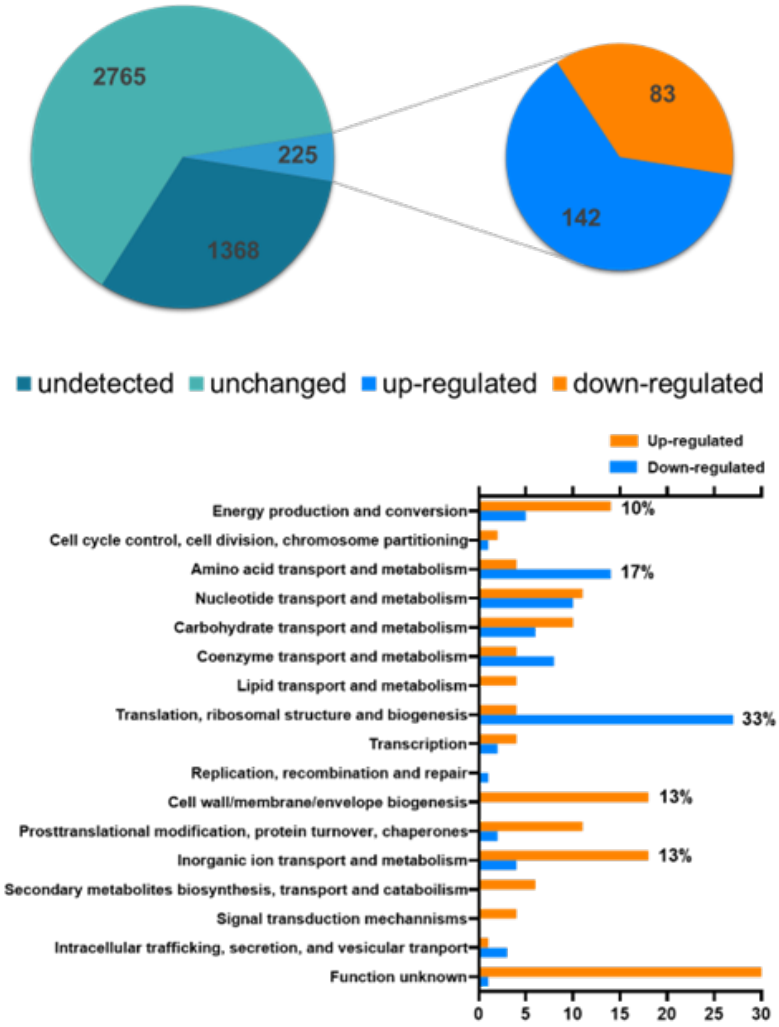

Figure S3. Quantitative proteomic analysis of *E. coli* MG1655 in response to acute Pi depletion.

Pie chart of total and differentially expressed proteins detected by LC-MS/MS analysis in *E. coli* MG1655 cells subjected to Pi depletion for 3 hours, relative to cells under Pi sufficient conditions. Red and blue colors represent significantly upregulated and downregulated proteins, respectively. Clusters of Orthologous Groups (COG) functional categories of differentially expressed proteins in *E. coli* MG1655 in response to Pi depletion. Red and blue colors represent significantly upregulated and downregulated proteins, respectively.

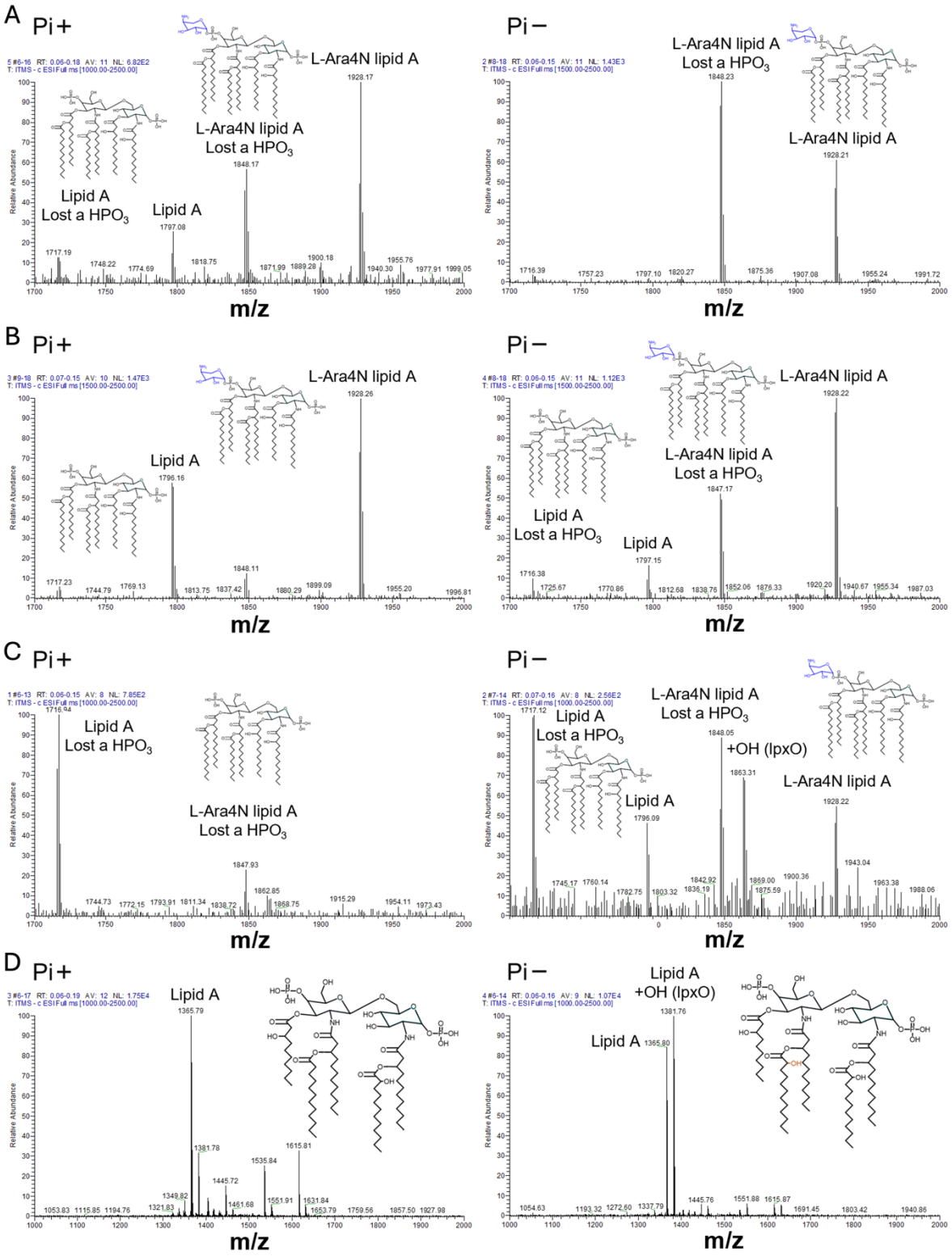

Figure S4. The ratio of L-Ara-4N modified Lipid A molecule increases in *E. coli* O157, *E. coli* UTI-3, *S.* Typhimurium ATCC14028 and *P. aeruginosa* PAO1 cells subjected to Pi depletion.

1215 (**A**) ESI-MS spectra of lipid A molecules extracted from *E. coli* O157 cells following acute Pi-
1216 starvation treatment (Pi-, 0 mM) (right) compared to the group without treatment (Pi+, 1.32 mM)
1217 (left). Peaks correspond to native lipid A lost a HPO_3 (1718), native lipid A (1798), L-Ara-4N
1218 modified lipid A lost a HPO_3 (1848) and L-Ara-4N modified lipid A (1928) are shown. (**B**) ESI-MS
1219 spectra of lipid A molecules extracted from *E. coli* UTI-3 cells following acute Pi-starvation
1220 treatment (Pi-, 0 mM) (right) compared to the group without treatment (Pi+, 1.32 mM) (left). Peaks
1221 correspond to native lipid A lost a HPO_3 (1718), native lipid A (1798), L-Ara-4N modified lipid A lost
1222 a HPO_3 (1848) and L-Ara-4N modified lipid A (1928) are shown. (**C**) ESI-MS spectra of lipid A
1223 molecules extracted from *S.* Typhimurium ATCC14028 cells following acute Pi-starvation
1224 treatment (Pi-, 0 mM) (right) compared to the group without treatment (Pi+, 1.32 mM) (left). Peaks
1225 correspond to native lipid A lost a HPO_3 (1718), native lipid A (1798), L-Ara-4N modified lipid A lost
1226 a HPO_3 (1848), L-Ara-4N and -OH modified lipid A lost a HPO_3 (1863) and L-Ara-4N modified lipid
1227 A (1928) are shown. (**D**) ESI-MS spectra of lipid A molecules extracted from PAO1 cells following
1228 acute Pi-starvation treatment (Pi-, 0 mM) (right) compared to the group without treatment (Pi+,
1229 1.32 mM) (left). Peaks correspond to hydroxylated lipid A lost a HPO_3 (1366), di-hydroxylated lipid
1230 A lost a HPO_3 (1382) are shown.

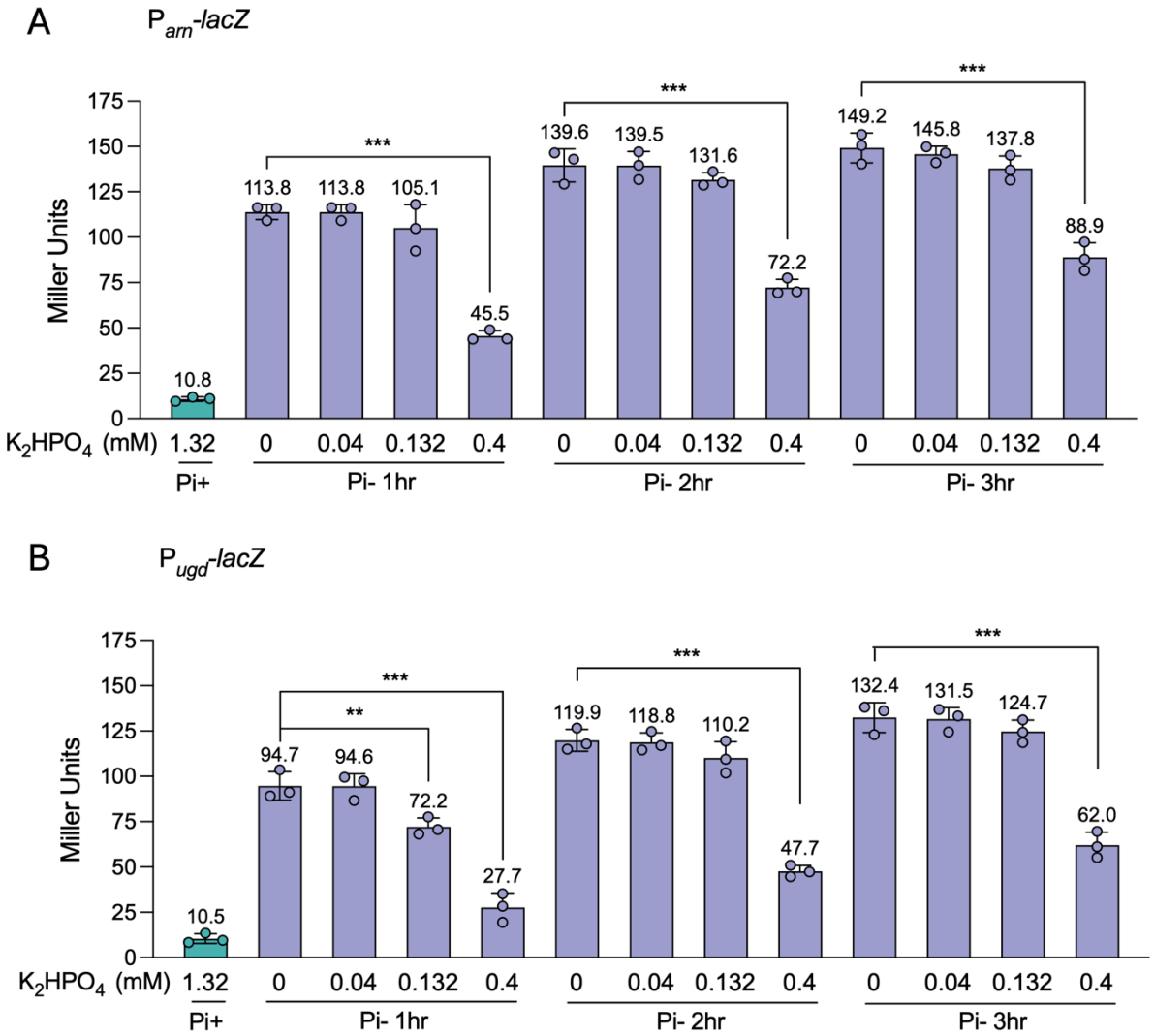

Figure S5. P*arn* and P*ugd* promoter activities in *E. coli* MG1655 during Pi depletion supplemented with different concentration of Pi.

(A) β-galactosidase activities of P_{arn}-*lacZ* in MG1655 Δ*lacZ* cells following Pi-starvation treatment with different concentration of Pi (Pi-, 0-0.4 mM) compared to the group without treatment (Pi+, 1.32 mM).

(B) β-galactosidase activities of P_{ugd}-*lacZ* in MG1655 Δ*lacZ* cells following Pi-starvation treatment with different concentration of Pi (Pi-, 0-0.4 mM) compared to the group without treatment (Pi+, 1.32 mM).

1240 Error bars represent the standard deviation of at least three independent experiments. Statistical

1241 significance was determined using one-way ANOVA followed by Dunnett's multiple comparisons

1242 test. Significance levels are indicated as follows: *$p < 0.05$; **$p < 0.01$; ***$p < 0.001$.

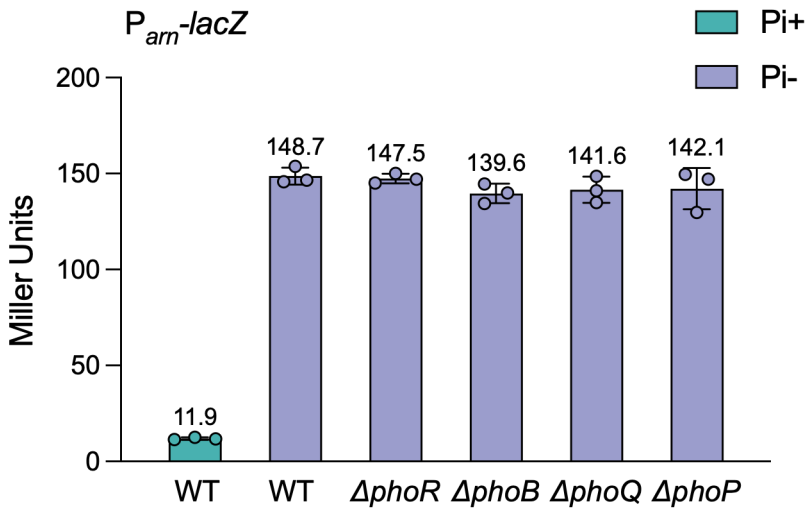

Figure S6. Up-regulation of *arn* genes during Pi depletion is independent of PhoBR and PhoPQ TCS in *E. coli* MG1655.

β-galactosidase activities of P_{ugd}-*lacZ* in MG1655 Δ*lacZ* parent and isogenic Δ*pmrB,* Δ*pmrA,* Δ*phoB* and Δ*phoR* mutants following acute Pi-starvation treatment (Pi-, 0 mM) compared to the group without treatment (Pi+, 1.32 mM).

Error bars represent the standard deviation of at least three independent experiments. Statistical significance was determined using one-way ANOVA followed by Dunnett's multiple comparisons test. Significance levels are indicated as follows: *$p < 0.05$; **$p < 0.01$; ***$p < 0.001$.

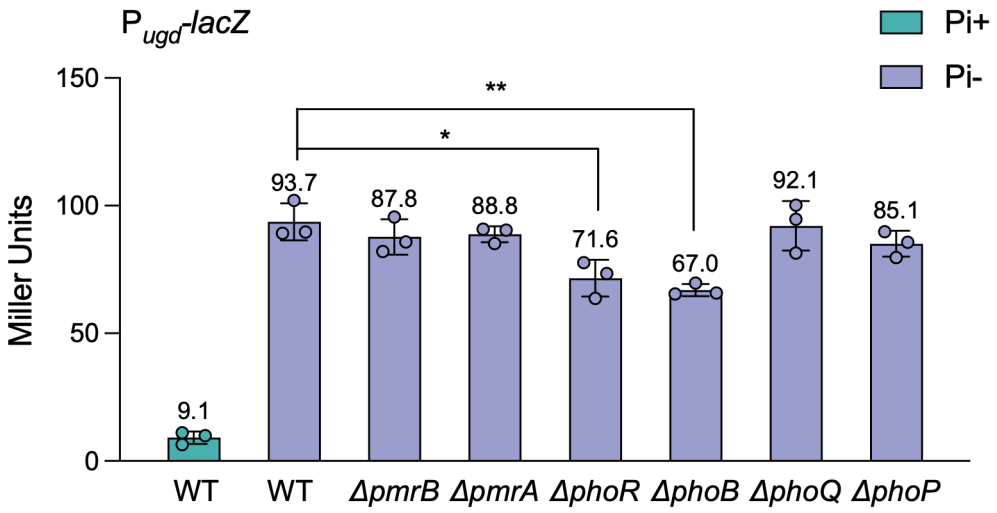

Figure S7. Up-regulation of *ugd* gene during Pi depletion is independent of PmrAB and PhoPQ TCS, but partially dependent on PhoBR TCS in *E. coli* MG1655.

β-galactosidase activities of P_{arn}-*lacZ* in MG1655 Δ*lacZ* parent and isogenic Δ*phoR,* Δ*phoB,* Δ*phoP* and Δ*phoQ* mutants following acute Pi-starvation treatment (Pi-, 0 mM) compared to the group without treatment (Pi+, 1.32 mM).

Error bars represent the standard deviation of at least three independent experiments. Statistical significance was determined using one-way ANOVA followed by Dunnett's multiple comparisons test. Significance levels are indicated as follows: *$p < 0.05$; **$p < 0.01$; ***$p < 0.001$.

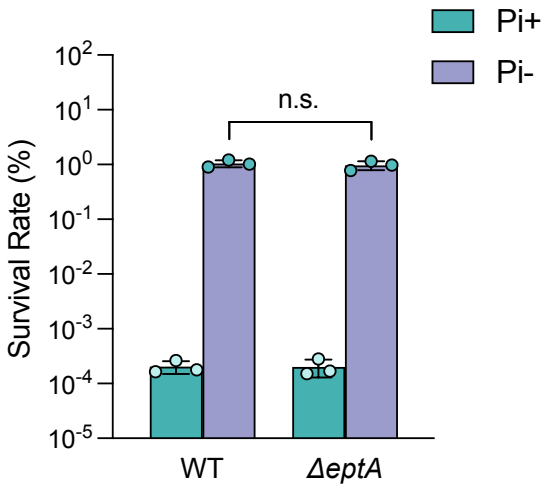

Figure S8. Pi depletion induced polymyxin tolerance is not affected in *eptA* deletion strain. Survival of *E. coli* MG1655 parent and isogenic ΔeptA mutant exposed 1-hour to polymyxin B (4 μg/ml) following acute Pi-starvation treatment (Pi-, 0 mM) compared to the group without treatment (Pi+, 1.32 mM).

Error bars represent the standard deviation of at least three independent experiments. Statistical significance was determined using two-tailed Student's t-test. Significance levels are indicated as follows: *$p < 0.05$; **$p < 0.01$; ***$p < 0.001$.

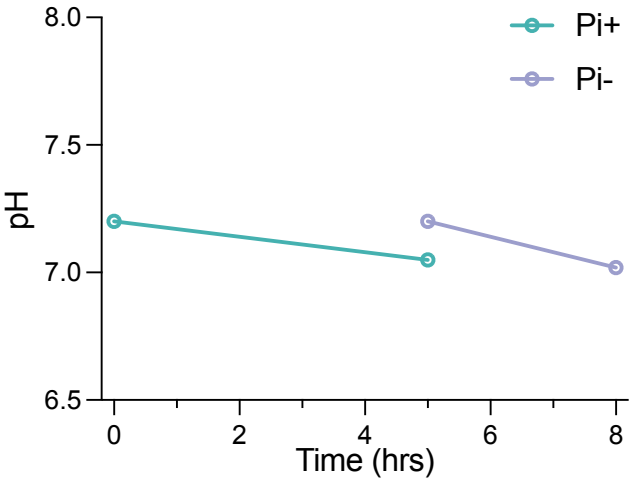

1271

1272 **Figure S9. pH of spent medium of *E. coli* MG1655 after 5hrs Pi sufficient growth and after**

1273 **3hrs Pi depletion treatment.**

1274 pH of the medium before bacteria inoculating and pH of the spent medium after 5hrs Pi sufficient

1275 growth or 3hrs Pi depletion treatment were measured.

1276 Error bars represent the standard deviation of at least three independent experiments.

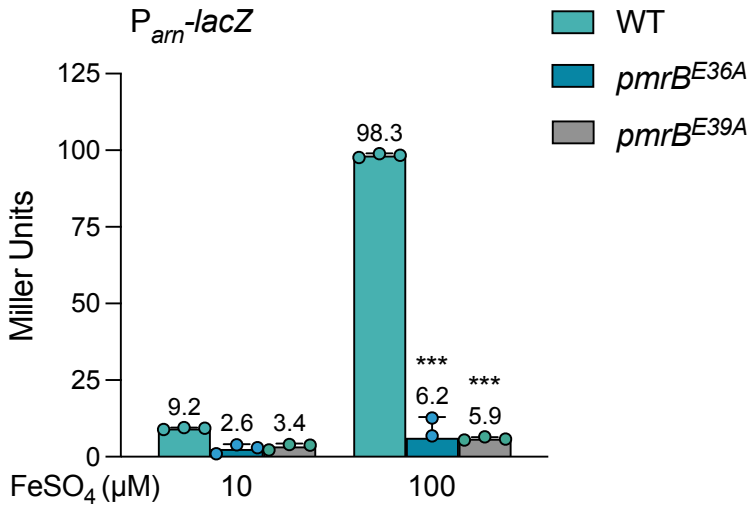

Figure S10. E36A and E39A mutation abolish the Fe^{3+} signaling capacity of PmrA.

β-galactosidase activities of P_{arn}-*lacZ* in MG1655 Δ*lacZ* parent and isogenic *pmrB*^{E36A}, *pmrB*^{E39A} mutants growth under MOPS minimal medium supplemented with different concentration of $FeSO_4$.

Error bars represent the standard deviation of at least three independent experiments. Statistical significance was determined using two-way ANOVA followed by Dunnett's multiple comparisons test. Significance levels are indicated as follows: *$p < 0.05$; **$p < 0.01$; ***$p < 0.001$.

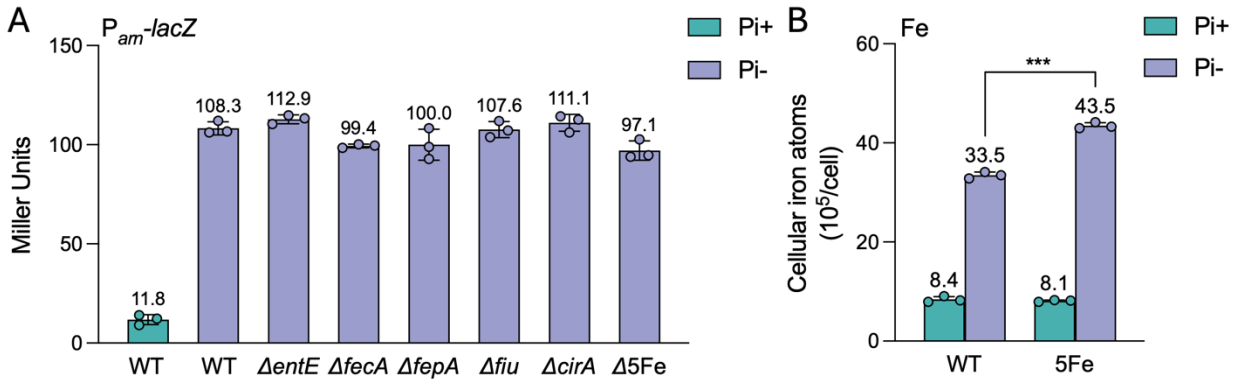

Figure S11. Deletion of canonical Fe^{3+} up-take genes does not affect the activation of PmrAB system and increase of Fe mobilization to *E. coli* cell during Pi depletion.

(**A**) β-galactosidase activities of P_{am}-*lacZ* in MG1655 Δ*lacZ* parent and isogenic Δ*fecA*, Δ*fepA*, Δ*entE*, Δ*fiu*, Δ*cirA*, and Δ5Fe (Δ*fecA*Δ*fepA*Δ*entE*Δ*fiu*Δ*cirA*) mutants following acute Pi-starvation treatment (Pi-, 0 mM) compared to the group without treatment (Pi+, 1.32 mM).

(**B**) Fe contents in *E. coli* MG1655 parent and isogenic Δ*fecA* Δ*fepA* Δ*entE* Δ*fiu* Δ*cirA* mutant following acute Pi-starvation treatment (Pi-, 0 mM) compared to the group without treatment (Pi+, 1.32 mM).

Error bars represent the standard deviation of at least three independent experiments. Statistical significance was determined using one-way ANOVA followed by Dunnett's multiple comparisons test for **A** and two-way ANOVA followed by Sidak's multiple comparisons test for **B**. Significance levels are indicated as follows: *$p < 0.05$; **$p < 0.01$; ***$p < 0.001$.

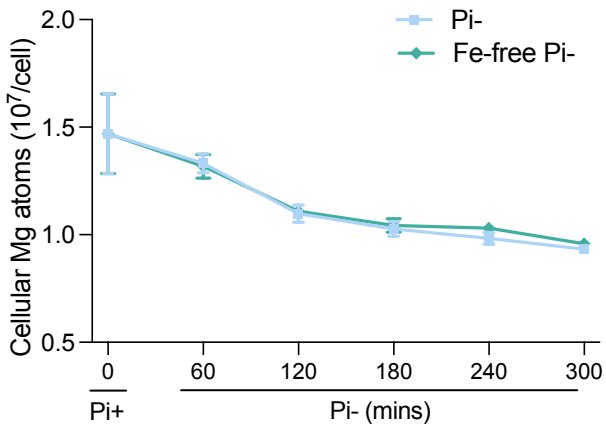

Figure S12. Decrease of cellular magnesium during Pi depletion is independent of Fe availability in medium.

Mg contents in *E. coli* MG1655 cell following Pi depletion treatment (0 Pi, 10 μM $FeSO_4$) or Fe-free Pi depletion treatment (0 Pi, 0 $FeSO_4$) at the indicated time points.

Error bars represent the standard deviation of at least three independent experiments.

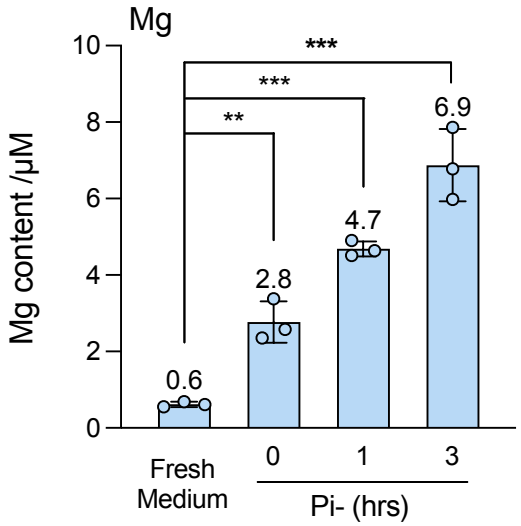

Figure S13. Magnesium disassociates from *E. coli* cells when subjected to Mg-free Pi-depleted medium.

Mg content in the spent medium during Mg-free Pi depletion treatment (0 Pi, 0 $MgCl_2$) at the indicated time points.

Error bars represent the standard deviation of at least three independent experiments. Statistical significance was determined using one-way ANOVA followed by Dunnett's multiple comparisons test. Significance levels are indicated as follows: *$p < 0.05$; **$p < 0.01$; ***$p < 0.001$.

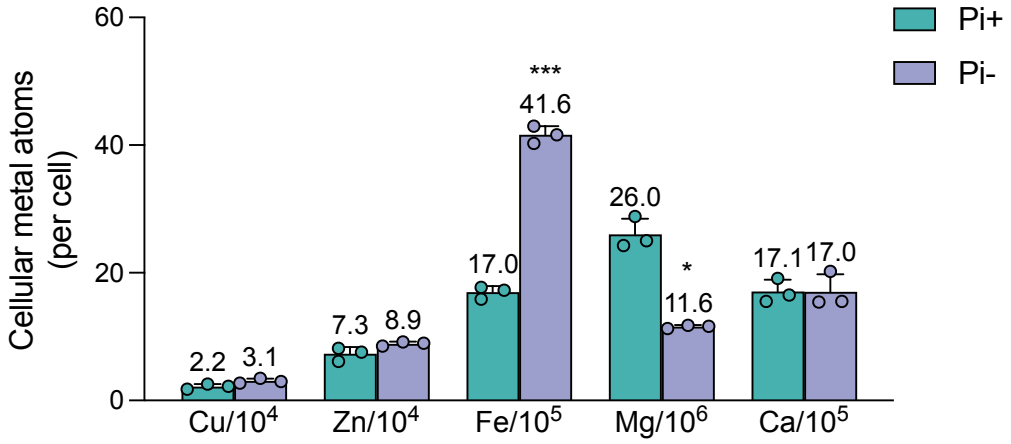

Figure S14. Cellular metal content in *P. aeruginosa* PAO1 cells with Pi depletion treatment and without Pi depletion treatment.

Cellular metal contents determined by ICP-MS in *P. aeruginosa* PAO1 cells following acute Pi-starvation treatment (Pi-, 0 mM) compared to the group without treatment (Pi+, 1.32 mM). Error bars represent the standard deviation of at least three independent experiments. Statistical significance was determined using two-tailed Student's t-test. Significance levels are indicated as follows: *$p < 0.05$; **$p < 0.01$; ***$p < 0.001$.

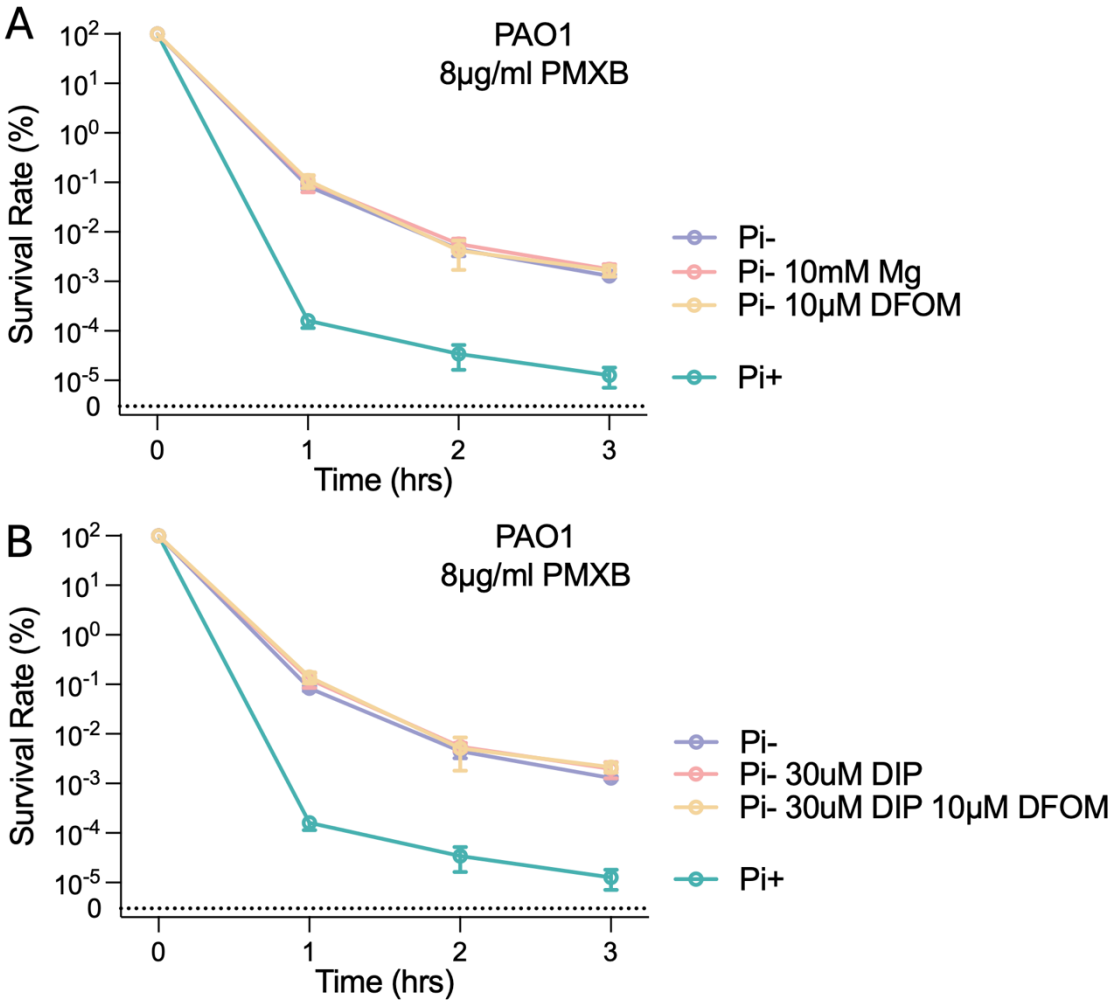

1321

1322 **Figure S15. Disruption of Mg and Fe signaling showed no effect on Pi depletion induced**

1323 **polymyxin resistance in *P. aeruginosa.***

1324 (A) Time-kill curves of *P. aeruginosa* PAO1 exposed to PMXB (8 μg/ml) following acute Pi-

1325 starvation treatment (Pi-, 0 mM Pi), Pi depletion treatment with excess Mg (Pi-, 0 mM Pi, 10mM

1326 $MgCl_2$) or Pi depletion treatment with iron chelator (Pi-, 0 mM Pi, 10 μM DFOM) compared to the

1327 group without treatment (Pi+, 1.32 mM Pi).

1328 (B) Time-kill curves of *P. aeruginosa* PAO1 exposed to PMXB (8 μg/ml) following acute Pi-

1329 starvation treatment (Pi-, 0 mM Pi), Pi depletion treatment with Fe^{2+} chelator (Pi-, 0 mM Pi, 30 μM

1330 DIP) or Pi depletion treatment with both Fe^{2+} and Fe^{3+}chelator (Pi-, 0 mM Pi, 30 μM DIP, 10 μM

1331 DFOM) compared to the group without treatment (Pi+, 1.32 mM Pi).

1332 Error bars represent the standard deviation of at least three independent experiments. Statistical

1333 significance was determined using one-way ANOVA followed by Dunnett's multiple comparisons

1334 test. Significance levels are indicated as follows: *$p < 0.05$; **$p < 0.01$; ***$p < 0.001$.

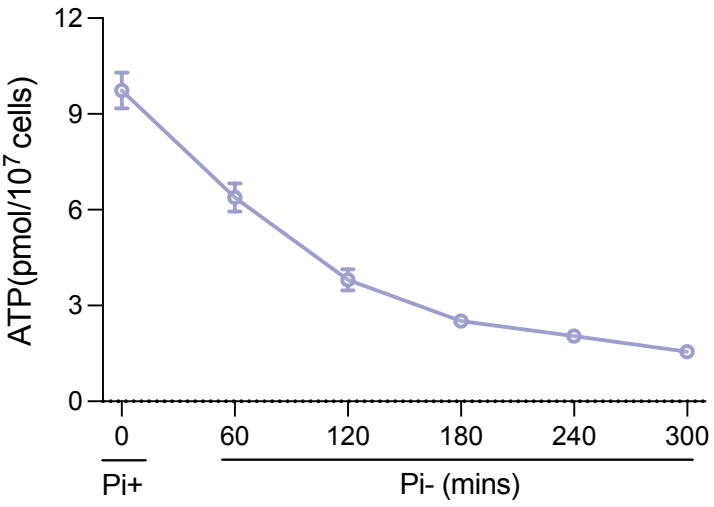

1335

1336 **Figure S16. Cellular ATP level in *E. coli* MG1655 cells continuously decrease during Pi**

1337 **depletion.**

1338 Cellular ATP levels in *E. coli* MG1655 cells following Pi depletion treatment at the specified time

1339 points. Error bars represent the standard deviation of at least three independent experiments.

1340

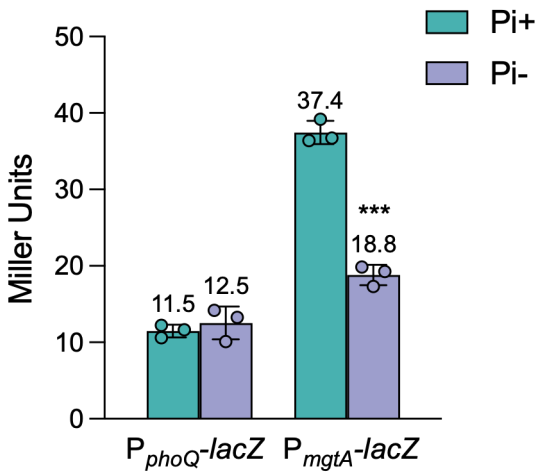

Figure S17. Lack of upregulation of P*phoQ* and P*mgtA* promoter activities indicates that the PhoPQ TCS is not activated during Pi depletion in *E. coli* MG1655.

β-galactosidase activities of P_{phoQ}-*lacZ* and P_{mgtA}-*lacZ* in MG1655 Δ*lacZ* parent following acute Pi-starvation treatment (Pi-, 0 mM) compared to the group without treatment (Pi+, 1.32 mM). Error bars represent the standard deviation of at least three independent experiments. Statistical significance was determined using two-tailed Student's t-test. Significance levels are indicated as follows: *$p < 0.05$; **$p < 0.01$; ***$p < 0.001$.

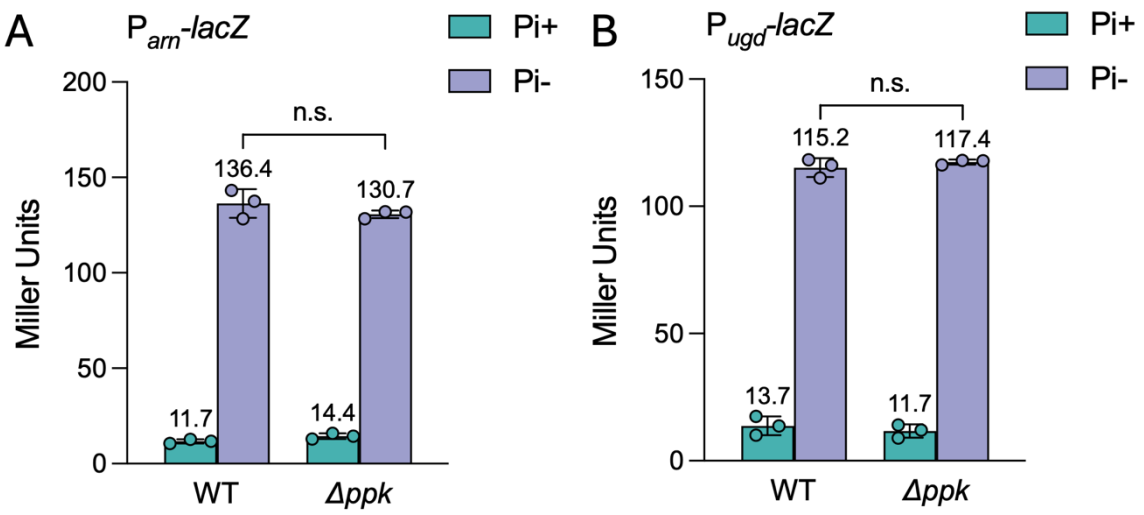

Figure S18. Up-regulation of both P*arn* and P*ugd* promoter activities during Pi depletion are not affected in *ppk* deletion strain.

(A) β-galactosidase activities of P_{arn}-*lacZ* in MG1655 Δ*lacZ* parent and isogenic Δ*ppk* mutant following acute Pi-starvation treatment (Pi-, 0 mM) compared to the group without treatment (Pi+, 1.32 mM).

(B) β-galactosidase activities of P_{ugd}-*lacZ* in MG1655 Δ*lacZ* parent and isogenic Δ*ppk* mutant following acute Pi-starvation treatment (Pi-, 0 mM) compared to the group without treatment (Pi+, 1.32 mM).

Error bars represent the standard deviation of at least three independent experiments. Statistical significance was determined using two-way ANOVA followed by Tukey's multiple comparisons test. Significance levels are indicated as follows: *$p < 0.05$; **$p < 0.01$; ***$p < 0.001$.

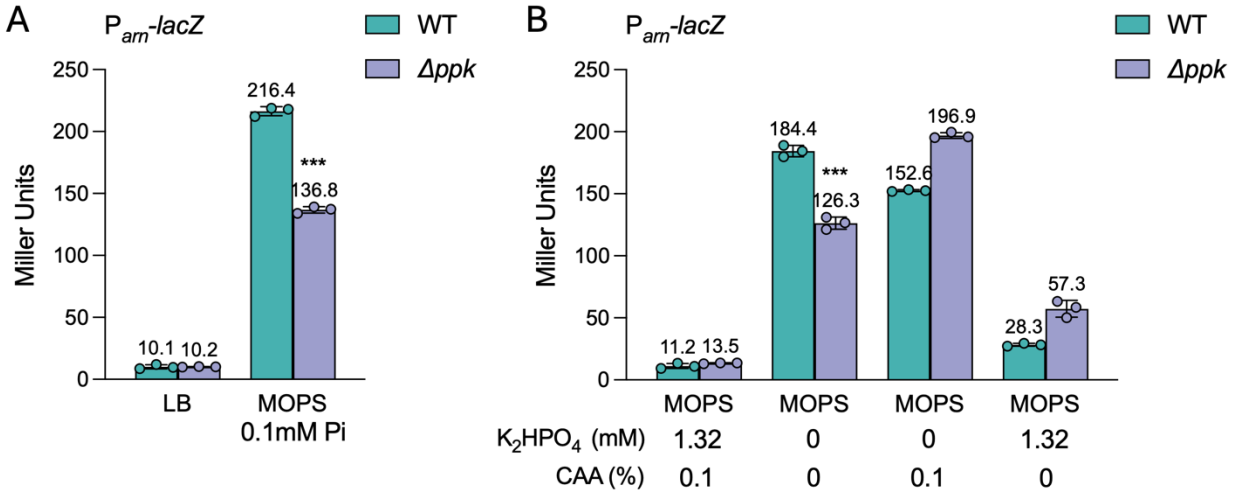

Figure S19. Pi depletion, amino acid depletion, and combined Pi–amino acid stress upregulate P*arn* promoter activity, while *ppk* deletion only attenuates upregulation under combined stress.

(A) β-galactosidase activities of P_{arn}-*lacZ* in MG1655 Δ*lacZ* parent and isogenic Δ*ppk* mutant following acute nutrients downshift (MOPS 0.1 mM Pi) compared to the group without treatment (LB). Error bars represent the standard deviation of at least three independent experiments. Statistical significance was determined using two-way ANOVA followed by Tukey's multiple comparisons test.

(B) β-galactosidase activities of P_{arn}-*lacZ* in MG1655 Δ*lacZ* parent and isogenic Δ*ppk* mutant following Pi depletion treatment (MOPS 0 Pi, 0.1% CAA), amino acid depletion treatment (MOPS 1.32 mM Pi, 0 CAA) and combined Pi–amino acid stress treatment (MOPS 0 Pi, 0 CAA) compared to the group without treatment (MOPS 1.32 mM Pi, 0.1% CAA).

Error bars represent the standard deviation of at least three independent experiments. Statistical significance was determined using two-way ANOVA followed by Tukey's multiple comparisons test. Significance levels are indicated as follows: *$p < 0.05$; **$p < 0.01$; ***$p < 0.001$.

1378 **Table S1.** Minimum inhibitory concentrations (MICs) of strains in MOPS minimal medium

Strain	PMXB (ug/ml)
MG1655	0.5
O157	1
UTI-1	0.5
UTI-3	1
UTI-4	1
UTI-5	1
PAO1	0.5
ATCC 14028	2

1379

1380 **Table S2.** Proteins identified to be different expressed in *E. coli* MG1655 growing under Pi

1381 sufficient and depletion conditions

prot_desc	id	log2FoldChange	padj
argF	sp|P06960|OTC2_ECOLI	-Inf	3.42E-18
gatZ	sp|P0C8J8|GATZ_ECOLI	-Inf	3.77E-09
fis	sp|P0A6R3|FIS_ECOLI	-Inf	2.78E-08
secY	sp|P0AGA2|SECY_ECOLI	-Inf	0.000159211
kgtP	sp|P0AEX3|KGTP_ECOLI	-Inf	0.001647533
gatC	sp|P69831|PTKC_ECOLI	-Inf	0.002435201
cysC	sp|P0A6J1|CYSC_ECOLI	-Inf	0.003341414
znuC	sp|P0A9X1|ZNUC_ECOLI	-Inf	0.025826417
rffH	sp|P61887|RMLA2_ECOLI	-Inf	0.036760697
cysD	sp|P21156|CYSD_ECOLI	-5.525585778	1.38E-11
mnmG	sp|P0A6U3|MNMG_ECOLI	-4.77187114	0.003253389
argA	sp|P0A6C5|ARGA_ECOLI	-4.649638457	2.18E-06
yhjE	sp|P37643|YHJE_ECOLI	-4.500028599	0.005992816
yegQ	sp|P76403|YEGQ_ECOLI	-4.482584177	0.015352456
cysN	sp|P23845|CYSN_ECOLI	-3.927062955	7.22E-14
pncB	sp|P18133|PNCB_ECOLI	-3.639270989	6.73E-05
fbp	sp|P0A993|F16PA_ECOLI	-3.600157407	0.023396164
moaA	sp|P30745|MOAA_ECOLI	-3.529794204	0.018342621

rpmC	sp|P0A7M6|RL29_ECOLI	-3.142935813	1.68E-07
ilvN	sp|P0ADF8|ILVN_ECOLI	-3.08821322	0.03765939
aroP	sp|P15993|AROP_ECOLI	-2.833642328	0.021648588
deaD	sp|P0A9P6|DEAD_ECOLI	-2.695068638	0.006647318
ilvB	sp|P08142|ILVB_ECOLI	-2.690257592	1.41E-07
asnA	sp|P00963|ASNA_ECOLI	-2.66746299	0.015909254
ptsG	sp|P69786|PTGCB_ECOLI	-2.510708646	0.000188954
rpmD	sp|P0AG51|RL30_ECOLI	-2.495454148	8.47E-09
ykgM	sp|P0A7N1|RL31B_ECOLI	-2.483011177	0.00644327
gatB	sp|P37188|PTKB_ECOLI	-2.418194429	0.035274735
cs	sp|P0A972|CSPE_ECOLI	-2.352007644	4.54E-08
metA	sp|P07623|META_ECOLI	-2.317452293	0.000139049
der	sp|P0A6P5|DER_ECOLI	-2.267771633	0.0102137
potA	sp|P69874|POTA_ECOLI	-2.183307337	0.03275735
leuA	sp|P09151|LEU1_ECOLI	-1.998105409	1.07E-08
glf	sp|P37747|GLF_ECOLI	-1.97691323	0.029751
tr	sp|P00895|TRPE_ECOLI	-1.943830992	0.005678046
miaB	sp|P0AEI1|MIAB_ECOLI	-1.92205685	0.004244044
pntB	sp|P0AB67|PNTB_ECOLI	-1.852085802	9.85E-06
purF	sp|P0AG16|PUR1_ECOLI	-1.826541229	4.76E-05
lepA	sp|P60785|LEPA_ECOLI	-1.791966706	0.01657399

gatY	sp|P0C8J6|GATY_ECOLI	-1.776699008	0.000182727
purT	sp|P33221|PURT_ECOLI	-1.764435997	0.000643699
prfC	sp|P0A7I4|RF3_ECOLI	-1.76312872	0.012506321
ybiC	sp|P30178|YBIC_ECOLI	-1.727397747	0.01941163
rpsH	sp|P0A7W7|RS8_ECOLI	-1.723379737	2.80E-10
purM	sp|P08178|PUR5_ECOLI	-1.678278829	0.003764
cyoA	sp|P0ABJ1|CYOA_ECOLI	-1.663437618	0.006838543
metL	sp|P00562|AK2H_ECOLI	-1.661017127	0.00181135
leuC	sp|P0A6A6|LEUC_ECOLI	-1.653771358	6.45E-06
pntA	sp|P07001|PNTA_ECOLI	-1.595004247	7.61E-08
trxB	sp|P0A9P4|TRXB_ECOLI	-1.571960722	0.002958769
metH	sp|P13009|METH_ECOLI	-1.565084962	0.000869601
metC	sp|P06721|METC_ECOLI	-1.510217214	0.025144896
rpmF	sp|P0A7N4|RL32_ECOLI	-1.498744569	0.000469522
gyrA	sp|P0AES4|GYRA_ECOLI	-1.448436432	7.72E-05
rpsR	sp|P0A7T7|RS18_ECOLI	-1.418043759	3.03E-05
rpmG	sp|P0A7N9|RL33_ECOLI	-1.381024188	0.006747605
purH	sp|P15639|PUR9_ECOLI	-1.376402854	0.000114658
argI	sp|P04391|OTC1_ECOLI	-1.37321011	0.000772873
rnb	sp|P30850|RNB_ECOLI	-1.364231063	0.003951903
rplT	sp|P0A7L3|RL20_ECOLI	-1.361561823	7.98781E-05

cysS	sp|P21888|SYC_ECOLI	-1.352510933	0.018153582
metK	sp|P0A817|METK_ECOLI	-1.28929395	0.000291382
sdhA	sp|P0AC41|SDHA_ECOLI	-1.284366661	8.12E-05
ydjN	sp|P77529|YDJN_ECOLI	-1.282130778	0.012801159
pyrD	sp|P0A7E1|PYRD_ECOLI	-1.24642368	0.017272295
rpsM	sp|P0A7S9|RS13_ECOLI	-1.231500265	4.82E-05
rpsC	sp|P0A7V3|RS3_ECOLI	-1.228519333	5.14E-06
rplU	sp|P0AG48|RL21_ECOLI	-1.200353979	0.000935979
pliG	sp|P76002|PLIG_ECOLI	-1.192616084	0.023769411
rplB	sp|P60422|RL2_ECOLI	-1.160209361	1.29E-05
rpsA	sp|P0AG67|RS1_ECOLI	-1.154439475	2.19E-06
rplS	sp|P0A7K6|RL19_ECOLI	-1.140490911	0.042048579
rpsT	sp|P0A7U7|RS20_ECOLI	-1.136468494	0.000373058
thrA	sp|P00561|AK1H_ECOLI	-1.131400346	7.55E-06
thrS	sp|P0A8M3|SYT_ECOLI	-1.130800143	0.017957548
rplR	sp|P0C018|RL18_ECOLI	-1.127973054	0.000234204
rplX	sp|P60624|RL24_ECOLI	-1.108686244	0.000297915
aceB	sp|P08997|MASY_ECOLI	-1.103226647	7.72E-05
aroA	sp|P0A6D3|AROA_ECOLI	-1.074448834	0.048313271
rplI	sp|P0A7R1|RL9_ECOLI	-1.074352178	3.31E-05
rplK	sp|P0A7J7|RL11_ECOLI	-1.030031069	0.000940436

argH	sp|P11447|ARLY_ECOLI	-1.029621386	0.010350803
cspC	sp|P0A9Y6|CSPC_ECOLI	-1.010776163	0.00524746
gpmA	sp|P62707|GPMA_ECOLI	1.007836346	0.000278112
gmhA	sp|P63224|GMHA_ECOLI	1.02030343	0.027607596
luxS	sp|P45578|LUXS_ECOLI	1.049588806	0.000506408
rpiA	sp|P0A7Z0|RPIA_ECOLI	1.052561101	0.01318169
pgi	sp|P0A6T1|G6PI_ECOLI	1.065800857	0.000188954
pykF	sp|P0AD61|KPYK1_ECOLI	1.081019653	2.73E-05
mlaC	sp|P0ADV7|MLAC_ECOLI	1.117643099	0.006345313
yfiF	sp|P0AGJ5|YFIF_ECOLI	1.128896995	0.03275735
uspG	sp|P39177|USPG_ECOLI	1.143746641	0.03765939
pgl	sp|P52697|6PGL_ECOLI	1.167828441	0.01318169
deoC	sp|P0A6L0|DEOC_ECOLI	1.174516518	0.018153582
grxB	sp|P0AC59|GLRX2_ECOLI	1.178432467	0.000732045
fbaB	sp|P0A991|ALF1_ECOLI	1.197658464	7.99E-05
adhE	sp|P0A9Q7|ADHE_ECOLI	1.201151692	3.88E-07
degP	sp|P0C0V0|DEGP_ECOLI	1.206061871	0.000278112
tas	sp|P0A9T4|TAS_ECOLI	1.219282681	0.036014767
katG	sp|P13029|KATG_ECOLI	1.220074858	7.01E-05
ribC	sp|P0AFU8|RISA_ECOLI	1.272415628	0.030285161
pmbA	sp|P0AFK0|PMBA_ECOLI	1.273270833	0.007784421

ftnA	sp|P0A998|FTNA_ECOLI	1.301974436	0.010044367
moaB	sp|P0AEZ9|MOAB_ECOLI	1.314241161	0.001746554
wrbA	sp|P0A8G6|NQOR_ECOLI	1.34050881	4.33E-06
hdhA	sp|P0AET8|HDHA_ECOLI	1.365397414	0.014224302
yahK	sp|P75691|YAHK_ECOLI	1.380128931	0.000137547
acnA	sp|P25516|ACNA_ECOLI	1.381383706	7.69E-05
sbp	sp|P0AG78|SUBI_ECOLI	1.410886097	0.001647533
degQ	sp|P39099|DEGQ_ECOLI	1.437968753	0.005431624
tktB	sp|P33570|TKT2_ECOLI	1.45986506	7.28E-07
yjgA	sp|P0A8X0|YJGA_ECOLI	1.470361111	0.0375636
glgP	sp|P0AC86|PHSG_ECOLI	1.489480956	0.004703968
yggE	sp|P0ADS6|YGGE_ECOLI	1.497996423	9.00E-05
mtlD	sp|P09424|MTLD_ECOLI	1.508297143	0.007422869
cbpA	sp|P36659|CBPA_ECOLI	1.520821408	0.040987772
deoB	sp|P0A6K6|DEOB_ECOLI	1.533048098	8.38E-05
ybjP	sp|P75818|YBJP_ECOLI	1.536131134	0.007427731
ybaY	sp|P77717|YBAY_ECOLI	1.541925932	0.00084693
tdcE	sp|P42632|TDCE_ECOLI	1.549713435	0.000108916
thiF	sp|P30138|THIF_ECOLI	1.58507647	0.00235383
hdeB	sp|P0AET2|HDEB_ECOLI	1.585194293	0.001902541
tpiA	sp|P0A858|TPIS_ECOLI	1.585411082	9.28E-09

uspE	sp|P0AAC0|USPE_ECOLI	1.605682754	0.000278112
rraA	sp|P0A8R0|RRAA_ECOLI	1.607904489	0.000417551
yeaY	sp|P0AA91|YEAY_ECOLI	1.609759679	0.001461256
nagD	sp|P0AF24|NAGD_ECOLI	1.651426571	0.020565443
slp	sp|P37194|SLP_ECOLI	1.661057589	0.000127411
osmC	sp|P0C0L2|OSMC_ECOLI	1.671087683	3.90E-06
ycfP	sp|P0A8E1|YCFP_ECOLI	1.676895218	0.000511934
acuI	sp|P26646|ACUI_ECOLI	1.680553338	0.001851227
pflB	sp|P09373|PFLB_ECOLI	1.700478434	9.87E-14
lpoB	sp|P0AB38|LPOB_ECOLI	1.721279546	0.000376072
clpB	sp|P63284|CLPB_ECOLI	1.727347175	1.23E-12
gstB	sp|P0ACA7|GSTB_ECOLI	1.748580068	0.001647533
slt	sp|P0AGC3|SLT_ECOLI	1.751322485	0.015251337
yggN	sp|P0ADS9|YGGN_ECOLI	1.768724665	0.049702565
loiP	sp|P25894|LOIP_ECOLI	1.795763405	0.012616436
pspA	sp|P0AFM6|PSPA_ECOLI	1.803047994	0.000834302
chrR	sp|P0AGE6|CHRR_ECOLI	1.829520642	0.00084693
gstA	sp|P0A9D2|GSTA_ECOLI	1.843282701	2.82E-06
msrA	sp|P0A744|MSRA_ECOLI	1.871059945	0.023254637
dps	sp|P0ABT2|DPS_ECOLI	1.8711205	1.92E-14
yghU	sp|Q46845|YGHU_ECOLI	1.947282377	0.000291495

lldD	sp|P33232|LLDD_ECOLI	1.949858867	0.035748827
yfcH	sp|P77775|YFCH_ECOLI	1.988861376	0.015909254
cdd	sp|P0ABF6|CDD_ECOLI	1.993269202	0.042932089
yeaG	sp|P0ACY3|YEAG_ECOLI	2.011516734	4.21E-11
pqiB	sp|P43671|PQIB_ECOLI	2.013507475	0.028681191
ygaU	sp|P0ADE6|YGAU_ECOLI	2.059465726	3.23E-14
blc	sp|P0A901|BLC_ECOLI	2.064974471	0.011100578
qorA	sp|P28304|QOR1_ECOLI	2.155671369	4.33E-07
curA	sp|P76113|CURA_ECOLI	2.175460559	0.010474873
bfr	sp|P0ABD3|BFR_ECOLI	2.180562547	1.56E-13
yegP	sp|P76402|YEGP_ECOLI	2.284730203	7.89E-10
ugd	sp|P76373|UDG_ECOLI	2.340441236	0.018153582
yceF	sp|P0A729|YCEF_ECOLI	2.382621181	0.040987772
yecA	sp|P0AD05|YECA_ECOLI	2.405409463	0.03275735
bepA	sp|P66948|BEPA_ECOLI	2.421711425	0.000774393
otsA	sp|P31677|OTSA_ECOLI	2.448868257	6.65E-08
katE	sp|P21179|CATE_ECOLI	2.50821371	2.35E-14
hchA	sp|P31658|HCHA_ECOLI	2.50879706	2.75E-12
dkgA	sp|Q46857|DKGA_ECOLI	2.649063918	1.64E-08
ybeL	sp|P0AAT9|YBEL_ECOLI	2.658797186	3.16E-08
ymdB	sp|P0A8D6|YMDB_ECOLI	2.671235984	0.024568779

fruB	sp|P69811|PTFAH_ECOLI	2.672541661	1.42E-05
ydbC	sp|P25906|YDBC_ECOLI	2.711914425	0.046758232
ynhG	sp|P76193|YNHG_ECOLI	2.733690087	3.31E-05
yciE	sp|P21363|YCIE_ECOLI	2.735728026	4.14E-05
ymbA	sp|P0AB10|YMBA_ECOLI	2.798163878	0.036198317
ydcL	sp|P64451|YDCL_ECOLI	2.82774542	2.04E-15
ldhA	sp|P52643|LDHD_ECOLI	2.837647013	2.28E-05
amn	sp|P0AE12|AMN_ECOLI	2.855927832	1.06E-13
yehZ	sp|P33362|YEHZ_ECOLI	2.946432256	0.017149234
mdtE	sp|P37636|MDTE_ECOLI	3.005567607	2.30E-05
gadB	sp|P69910|DCEB_ECOLI	3.026824738	1.75E-33
yhjG	sp|P37645|YHJG_ECOLI	3.114565954	0.004244044
gadC	sp|P63235|GADC_ECOLI	3.122545884	0.000234696
gadA	sp|P69908|DCEA_ECOLI	3.154673417	6.58E-36
ydhF	sp|P76187|YDHF_ECOLI	3.156625723	5.19E-05
yjgR	sp|P39342|YJGR_ECOLI	3.159652222	1.41E-12
yghA	sp|P0AG84|YGHA_ECOLI	3.175685027	1.40E-09
ycaC	sp|P21367|YCAC_ECOLI	3.185383669	2.44E-13
phoE	sp|P02932|PHOE_ECOLI	3.204721908	2.80E-10
ycgM	sp|P76004|YCGM_ECOLI	3.314835257	0.007920581
tam	sp|P76145|TAM_ECOLI	3.330887068	0.010474873

yhbO	sp|P45470|YHBO_ECOLI	3.335162899	0.000187361
phoR	sp|P08400|PHOR_ECOLI	3.473374236	0.001325039
mdaB	sp|P0AEY5|MDAB_ECOLI	3.504985139	1.26E-20
dkgB	sp|P30863|DKGB_ECOLI	3.638374711	5.12E-09
yniA	sp|P77739|YNIA_ECOLI	3.681925301	2.85E-07
gldA	sp|P0A9S5|GLDA_ECOLI	3.74947351	3.13E-05
phnD	sp|P16682|PHND_ECOLI	3.815420505	9.61E-10
ugpQ	sp|P10908|UGPQ_ECOLI	4.003964005	1.04E-06
ahr	sp|P27250|AHR_ECOLI	4.055942555	2.68E-05
pstS	sp|P0AG82|PSTS_ECOLI	4.113208109	3.15E-56
cysQ	sp|P22255|CYSQ_ECOLI	4.144617537	1.22E-07
glsA1	sp|P77454|GLSA1_ECOLI	4.234450197	0.024320745
yciF	sp|P21362|YCIF_ECOLI	4.316219533	0.000228764
ais	sp|P45565|AIS_ECOLI	4.363027397	0.02438333
kefG	sp|P0A756|KEFG_ECOLI	4.489497738	0.01318169
ydcS	sp|P76108|YDCS_ECOLI	4.581943058	0.009304996
phnB	sp|P16681|PHNB_ECOLI	4.606620186	4.21E-11
sodC	sp|P0AGD1|SODC_ECOLI	4.625310091	1.37E-05
arnA	sp|P77398|ARNA_ECOLI	4.698344251	1.36E-11
fic	sp|P20605|FIC_ECOLI	4.74532692	0.001647533
ugpB	sp|P0AG80|UGPB_ECOLI	4.789402823	1.62E-50

phoU	sp|P0A9K7|PHOU_ECOLI	4.829226009	7.34E-29
kdpC	sp|P03961|KDPC_ECOLI	4.927327983	0.001190624
pstB	sp|P0AAH0|PSTB_ECOLI	5.294764534	6.41E-25
yebE	sp|P33218|YEBE_ECOLI	5.774676565	1.18E-14
phoA	sp|P00634|PPB_ECOLI	5.790096911	7.32E-85
phoB	sp|P0AFJ5|PHOB_ECOLI	Inf	8.96E-35
arnB	sp|P77690|ARNB_ECOLI	Inf	8.99E-08
appA	sp|P07102|PPA_ECOLI	Inf	7.69E-05
yedP	sp|P76329|MPGP_ECOLI	Inf	7.72E-05
ugpC	sp|P10907|UGPC_ECOLI	Inf	0.000683993
arnC	sp|P77757|ARNC_ECOLI	Inf	0.008862011
yfcG	sp|P77526|YFCG_ECOLI	Inf	0.018153582
yraR	sp|P45469|YRAR_ECOLI	Inf	0.012911411
yhhA	sp|P0ADX7|YHHA_ECOLI	Inf	0.018724338
phnH	sp|P16686|PHNH_ECOLI	Inf	0.025826417
gspJ	sp|P45761|GSPJ_ECOLI	Inf	0.036463755
PmrA	sp|P30843|PMRA_ECOLI	Inf	0.037433165
alpA	sp|P33997|ALPA_ECOLI	Inf	0.037433165

1382

1383 **Table S3.** Bacteria strains used in this study.

Name	Description	Source
MG1655	*F- λ- ilvG- rfb-50 rph-1*	Lab collection
DH5α	*E. coli* F⁻ *endA1 glnV44 thi-1 recA1 relA1 gyrA96 deoR nupG purB20 φ80dlacZΔM15 Δ(lacZYA-argF)U169*, *hsdR17*($r_K^- m_K^+$), λ^-	Lab collection
Bl21 (DE3)	*E. coli* B F⁻ *ompT gal dcm lon hsdS*$_B$($r_B^- m_B^-$) [*malB*$^+$]$_{K-12}$(λ^S)	Lab collection
E. coli O157	EHEC, O157:H7	Clinical isolate from Queen Mary Hospital (HK)
UTI-1	UPEC isolated from UTI patients	Clinical isolate from Queen Mary Hospital (HK)
UTI-3	UPEC isolated from UTI patients	Clinical isolate from Queen Mary Hospital (HK)
UTI-4	UPEC isolated from UTI patients	Clinical isolate from Queen Mary Hospital (HK)
UTI-5	UPEC isolated from UTI patients	Clinical isolate from Queen Mary Hospital (HK)
Salmonella ATCC14028	*Salmonella* ATCC14028 wild type	Lab collection
P. aeruginosa	*P. aeruginosa* PAO1 wild type	Lab collection

PAO1

AY7010	MG1655 ArnB-3xFLAG	This study
AY0416	MG1655 Δ*lacZ::Km*^{R}	This study
AY4875	MG1655 Δ*arnT*:: *Km*^{R}	This study
AY4860	MG1655 Δ*arnB*:: *Km*^{R}	This study
AY4862	MG1655 Δ*ugd*:: *Km*^{R}	This study
AY4858	MG1655 Δp*mrB*:: *Km*^{R}	This study
AY4859	MG1655 Δ*pmrA*:: *Km*^{R}	This study
AY2741	MG1655 Δ*phoB*:: *Km*^{R}	This study
AY2742	MG1655 Δ*phoR*:: *Km*^{R}	This study
AY7011	MG1655 Δ*pmrB*:: *Km*^{R}*ΔlacZ*	This study
AY7012	MG1655 Δ*pmrA*:: *Km*^{R}*ΔlacZ*	This study
AY7013	MG1655Δ*phoB*:: *Km*^{R}*ΔlacZ*	This study
AY7014	MG1655Δ*phoR*:: *Km*^{R}*ΔlacZ*	This study
AY7015	MG1655 *ΔlacZ, pmrB*^{E36A}	This study
AY7016	MG1655 *ΔlacZ, pmrB*^{E39A}	This study
AY7017	MG1655 Δ*pmrA*	This study
AY7018	MG1655 *pmrB*^{E36A}	This study
AY7019	MG1655 *pmrB*^{E39A}	This study
AY7020	MG1655 Δ*fecA*	This study
AY7021	MG1655 Δ*fepA*	This study

AY7022	MG1655 Δ*entE*	This study
AY7023	MG1655 Δ*fiu*	This study
AY7024	MG1655 Δ*cirA*	This study
AY7025	MG1655 Δ*fecA* Δ*fepA* Δ*entE* Δ*fiu* Δ*cirA*	This study

1384

1385

1386 **Table S4.** Plasmids used in this study.

Name	Relevant characteristics	Source
pNN387	Single copy plasmid containing NotI and HindIII restriction sites before *lacZ*	Lab collection
pNN387(P_{arn}-*lacZ*)	Ligate promoter of *arn* into NotI/HindIII linearized pNN387	This study
pNN387(P_{ugd}-*lacZ*)	Ligate promoter of *ugd* into NotI/HindIII linearized pNN387	This study
pNN387(P_{phoQ}-*lacZ*)	Ligate promoter of *phoQ* into NotI/HindIII linearized pNN387	This study
pNN387(P_{mgtA}-*lacZ*)	Ligate promoter of *mgtA* into NotI/HindIII linearized pNN387	This study
pET28a-N	t7 promoter in pET-28a is replaced by araBad promoter	This study
pET28a-N-3xFLAG	C-terminal 6xHis tag in pET-28a-N is replaced by 3xFLAG tag	This study
pET-N-PmrA-6xHis	Ligate *pmrA* into NcoI/XhoI linearized pET-28a-N	This study
pET-N-PmrA-3xFLAG	Ligate *pmrA* into NcoI/XhoI linearized pET-28a-N-3xFLAG	This study
pET-N-PmrA137TAG-6xHis	Mutate G137 to TAG in pET28A-N-PmrA-6xHis	This study

pEVOL-CouA-RS	Plasmid expression CouA tRNA synthetase	Lab collection
pCAGO	Editing plasmid containing CRISPR-Cas9 and λ-red	Gift from Prof. Changhao Bi

1387